N 70 39914

STUDY OF INFRARED RADIATION FROM SEMICONDUCTOR DEVICES

ADVANCED KINETICS

COSTA MESA CALIFORNIA

CASE FILE COPY

STUDY OF INFRARED RADIATION FROM SEMICONDUCTOR DEVICES

FINAL TECHNICAL REPORT

Contract NAS12-2199

NATIONAL AERONAUTICS AND SPACE ADMINISTRATION
ELECTRONICS RESEARCH CENTER
CAMBRIDGE, MASSACHUSETTS

JUNE 10, 1970

TABLE OF CONTENTS

		PAGE
I)	INTRODUCTION	1
II)	RADIATIVE EMISSION FROM SEMICONDUCTORS	5
	A) GENERAL DISCUSSION OF THE PROBLEM	5
	B) RADIATION FROM DIRECT INTERBAND RECOMBINATION	7
	1) Semiconductor with Low Impurity Concentration . .	9
	2) Semiconductor with Low Excitation Level	10
	3) Heavily Doped Semiconductor	10
	4) Semiconductors with High Excitation Level.	11
	C) EVALUATION OF RECOMBINATION RATE	12
	D) RADIATION FROM INDIRECT TRANSITIONS (TRAPPING CENTERS)	16
	1) Case of Low Carrier Density Injection	19
	2) Case of Large Carrier Density Injection	20
	E) IMPACT RECOMBINATION MECHANISM	21
	1) High Excitation Level	22
	2) Low Excitation Level	23
	F) THERMAL RADIATION FROM SEMICONDUCTORS . . .	25
III)	RADIATIVE LOSSES DURING EMISSION	30
	A) REFRACTIVE LOSSES	30
	B) ABSORPTION LOSSES	32

TABLE OF CONTENTS
(Continued)

		PAGE
IV)	TRANSMISSION OF RADIATIVE SIGNAL	34
	A) TRANSMISSION THROUGH DIELECTRIC MEDIUM	34
	B) TRANSMISSION THROUGH LIGHTGUIDES	36
V)	EVALUATION OF RADIATION DETECTION PROBLEMS	40
VI)	DISCUSSION OF EXPERIMENTAL EFFORT	46
VII)	CALIBRATION OF INFRARED DETECTORS	49
VIII)	EXPERIMENTS ON RADIATION FROM SEMICONDUCTORS . .	51
	A) EXPERIMENTS WITHOUT SCREENING CAGE	51
	B) EXPERIMENTS INSIDE FARADAY SCREEN CAGE	53
IX)	CONCLUSIONS AND RECOMMENDATIONS	57
X)	REFERENCES	64

FIGURE 1 Refractive Indices for Germanium and Silicon in the Near Infrared

FIGURE 2 Absorption Coefficient K for Germanium and Silicon at 300°K

FIGURE 3 Recombination Rate in Germanium per Unit Frequency and Volume vs. $h\nu/kT = 300°K$

TABLE OF CONTENTS
(Continued)

FIGURE 4 Transmission of Plastic and Glass Fibers Between 0.4 - 2 μm

FIGURE 5 Transmission of Glass Fibers for Several Lengths Between 0.4 - 2 μm

FIGURE 6 Experimental Configuration with Dielectric Lightguide

FIGURE 7 Experimental Configuration with Metallic Lightguide and Dual Detector

FIGURE 8 Radiation from 2N1183 NPN Power Transistor with Current Modulation Function

FIGURE 9 Detected Radiation Signal from Junction of 2N1183 Transistor

FIGURE 10 Test Set-up for Measurement of Radiation from Semiconductors

FIGURE 11a Top View of NPN Power Transistor Type 2N1701
FIGURE 11b Enlarged Drawing of NPN-2N1701 with Scan Line Entered

FIGURE 12 Scan Across 2N1701 NPN Power Transistor

FIGURE 13 Numerically Controlled Stage Scan Across Emitter-Base Junction of NPN-2N1701 Power Transistor

FIGURE 14 Detected Radiation Signal vs Inclination Angle of Lightguide

FIGURE 15 Detected Radiation Signal vs Collector Current for NPN-2N1701 Power Transistor

FIGURE 16 Detected Radiation Signal vs Collector Voltage for NPN-2N1701 Power Transistor

FIGURE 17 Detected Radiation Signal vs Anode Current for RCA Triac 40430

TABLE I Calibration of PbS Detector

TABLE II Calibration of Ge:Hg Detector

The following personnel of Advanced Kinetics, Inc. have participated in the performance of this program

Dr. Ralph W. Waniek

Mr. Harold E. Miller

Mr. Roy Mollet

Mr. Anthony Soulias

Mr. John Yanos

Mr. Terrence L. Wolf

ACKNOWLEDGEMENTS

The technical staff of Advanced Kinetics, Inc. wishes to acknowledge the valuable guidance and the pertinent discussions of the problem provided during the course of this program by Mr. William W. Lurie, Technical Monitor and by Mr. C. W. Watt of the Electronic Research Center, National Aeronautics and Space Administration, Cambridge, Massachusetts.

1) INTRODUCTION

The possibility of conducting diagnostic studies of semiconducting devices by analysis of the radiation emitted under operating conditions is extremely enticing. The radiative output can be interpreted not only in terms of dissipative effects within the bulk of the device but also in terms of properties related to the charge carriers and to the electronic structure of the semiconductor. Thus, it is immediately evident that any diagnostic technique developed for this purpose must be based on a reliable theoretical model of the mechanism generating the radiation.

Two main classes of effects are expected to contribute to this radiative emission. The first category covers thermal emission. This component of the radiation is indicative for dissipative effects in the device and the profile of the emission is the result of local heat deposition and of thermal diffusion in the slab. The second mechanism is attributable to carrier recombination effects in the solid and hence this component is of non-thermal origin.

The central problem in this investigation concerns the differentiation between these two contributions and the evaluation of the radiative emission expected from a generalized slab of semiconducting material.

The thermal emission is easily described in terms of black body theory and of thermal heat flow in the medium. However, the treatment of radiation due to recombination effects is more complicated. The theory of the radiative recombination

in semiconductors was developed by Van Roosbroeck and Shockley[1], and many useful guidelines can be applied to this problem.

The two main contributing processes are direct recombination of electrons from the conduction band and holes from the valence band and the recombination through local centers (traps). Direct or interband recombination in pure semiconductors is a relatively small contribution. For the usual values of the forbidden bandwidth, $\Delta E \approx 1 - 2$ ev, the intensity of the radiative recombination (RR) is negligible. In effect, in germanium at room temperature (300°K) with $\Delta E = 0.7$ ev the RR lifetime is 0.75 sec, and for substances with a wider forbidden band this lifetime is even longer. On the other hand, in semiconductors with a narrow forbidden band the RR rate is high and the radiative mechanism may be the dominant source of energy dissipation. For example, in InSb at 300°K, $\Delta E = 0.18$ ev and the RR lifetime is only about 10^{-6} sec. The usual measured lifetime of the nonequilibrium carriers in germanium amounts to 10^{-3} to 10^{-4} sec. Thus, RR is not the main mechanism in germanium, but recombination through traps (TR) is the main factor. Only in heavily doped samples ($n_o = 10^{19}$ cm^{-3}), we find that RR competes with TR if the trap (local centers) concentration does not increase with the degree of doping. In silicon the situation is even more pronounced since $\Delta E = 1.1$ ev, $n_i = 1.4 \cdot 10^{10}/cm^3$ and $\tau_i = 3.5$ sec. The maximum value of the observed lifetime for silicon is 10^{-3} sec, and hence TR is still the main contributing factor.

The RR spectrum to be expected, for instance for germanium, is simply computed from the value of $h\nu/kT = 27.5$ (at room temperature), thus corresponding to a peak at $\lambda = 1.76\ \mu m$. In practice, a second peak is found at $1.52\ \mu m$, in a region where the absorption in germanium rises steeply due to direct phototransitions. The radiation maximum lies close to the fundamental absorption edge at $\lambda = 2.05\ \mu m$.

If the energy released upon recombination is not available directly in form of radiation, it will usually reappear in form of phonons (lattice vibrations). The recombination energy may be transferred first to a free carrier which then gradually transmits the same to the lattice by means of collisions. This process is know as impact recombination. Other processes involve transfer to plasmons (collective motion of free carriers) or to excitons. For the case of TR, an electron is first captured by a level of the local impurity center and then the same level captures also a hole.

If the carrier energy is degraded by these mechanisms into thermal energy, then the spectrum distribution will be described by equipartition theory and the radiant distribution will approach that of a black body.

The objectives of this program are to evaluate first the mechanism in terms of the most suitable descriptive model and subsequently, to study the radiation output from selected semiconductor geometries. Finally, the properties of the emitted radiation will be compared with those provided by the theoretical forecast

and guidelines will be offered for using this method as a practical diagnostic tool in solid state electronics.

II) RADIATIVE EMISSION FROM SEMICONDUCTORS

A) GENERAL DISCUSSION OF THE PROBLEM

The central problem of this research and development program is to identify and to forecast the radiation emitted by semiconductors under current passage. Of particular importance is the knowledge of the radiative contribution from the various generating mechanisms, the relative intensities, the spectral distributions and the dependence on current excitation.

We shall consider here three basic mechanisms for generation of radiation and we shall evaluate the relative contributions. These radiative modes include direct recombination of electrons from the conduction band and holes from the valence band (labelled here DR and RR for direct or radiative recombination), the recombination through local centers or traps (labelled here TR or trap radiation) and, finally, thermal radiation (ThR) which is due to the energy degradation of free carriers into phonon vibrations. The process of impact recombination is also discussed, since it leads to lattice excitation which should be detectable in the infrared.

Direct or interband recombination in pure semiconductors is generally a relatively small contribution. This statement needs, however, some qualifications. First of all, we should examine the value of the

forbidden bandwidth of the particular semiconductor. If the figure is on the order of 1 - 2 ev, then the intensity of the radiative recombination should be relatively negligible. On the other hand, if the figure is much smaller than 1 ev, the opposite holds and DR becomes a mechanism for substantial energy dissipation. From this viewpoint, the generation of recombination radiation in germanium and silicon is expected to be an insignificant contribution in pure materials.

The second qualification which must be applied concerns the degree of dopant concentration in the pure sample. This parameter yields an indication of the relative contribution of DR versus TR. In germanium, for instance, only in heavily doped samples with a concentration $n_o \approx 10^{19}$ cm^{-3} do we expect the DR lifetimes to become on the order of the TR lifetimes.

The third mode of energy dissipation entails a number of complex steps. In general, if DR or TR are not generated directly upon recombination, the energy will eventually reappear in form of phonons. One of the possible processes includes impact recombination in which the recombination energy is transferred in a first step to a free carrier which gradually interacts with the lattice and looses energy. More complex degradation involves collective motion of free carriers and the generation of excitons. The analytical evaluation of this case is reasonably complicated and only approximate estimates can be given for the expected contribution.

B) RADIATION FROM DIRECT INTERBAND RECOMBINATION

In the following, we shall present the pertinent features of direct interband recombination radiation. The descriptive theory has been given by van Roosbroeck and Shockley[1] and it can be used appropriately for the definition of this problem.

First of all, we expect direct interband recombination radiation to be identical in different samples of the same material. This entails that for the same electron and hole densities in the bands and for the same operating temperature, the emitted output should remain essentially constant. This is in contrast with trap radiation which could conceivably vary by appreciable amounts for different samples of the same material. Thus, from the viewpoint of diagnostic applicability in this program, it would be preferable to deal with DR rather than with TR in terms of the reliability of the forecast.

A second point to be stressed is the relative simplicity of the theoretical model for DR as opposed to the TR case. Direct radiative recombination, as shown by van Roosbroeck and Shockley, can be calculated simply from general thermodynamic considerations using experimental absorption data. However, for recombination through traps the theoretical calculations require a detailed knowledge of the microscopic mechanism and the descriptive parameters of electron or hole capture.

We should first examine the equilibrium situation. For this case, the rate of radiative recombination R_o is simply proportional to the densities of electrons and holes and the proportionality constant is the radiative recombination coefficient γ

$$R_o = \gamma n_o p_o = \gamma n_i^2 \tag{1}$$

Here n_o and p_o are the equilibrium concentrations of electrons and holes, respectively, and n_i is the concentration of carriers in an intrinsic semiconductor. Therefore γ is simply

$$\gamma = R_o/n_i^2 \tag{2}$$

The nonequilibrium case is of more basic interest here. If the energy distribution in the bands of the nonequilibrium populations is identical to that of the equilibrium populations, then the two cannot be distinguished and we can write the corresponding expressions for the rate of radiative recombination under nonequilibrium conditions

$$R = \gamma np = npR_o/n_i^2 \tag{3}$$

The non-equilibrium concentrations are related by

$$n = n_o + \Delta n$$

$$p = p_o + \Delta p \qquad (4)$$

$$n_i^2 = n_o p_o$$

We can now define the lifetimes of the radiating nonequilibrium populations of electrons and holes

$$\tau_n = \Delta n / (R - R_o) = \Delta n / \Delta R \qquad (5)$$

$$\tau_p = \Delta p / (R - R_o) = \Delta p / \Delta R \qquad (6)$$

and

$$\Delta R = R - R_o = R_o \frac{np - n_i^2}{n_i^2} \qquad (7)$$

We shall now focus on several cases of interest:

1) Semiconductor with Low Impurity Concentration

The simplest case entails a semiconductor of low impurity concentration for which the neutrality condition is expressed as $\Delta n = \Delta p$.

We obtain for ΔR and for the lifetime τ the following expressions.

$$\Delta R = \Delta R_o \frac{(n_o + p_o)\Delta n + (\Delta n)^2}{n_i^2} \tag{8}$$

$$\tau_n = \tau_p = \frac{1}{R_o} \frac{n_i^2}{(n_o + p_o) + \Delta n} \tag{9}$$

2) Semiconductor with Low Excitation Level

For a low excitation level, $(n_o + p_o) \gg \Delta n$, thus we can simplify the above expressions to

$$\Delta R = R_o \frac{(n_o + p_o)\Delta n}{n_i^2} \tag{10}$$

$$\tau_n = \tau_p = \frac{1}{R_o} \frac{n_i^2}{n_o + p_o} \tag{11}$$

In this regime, we have linear recombination since $\Delta R \propto \Delta n$.

3) Heavily Doped Semiconductor

For a heavily doped semiconductor, we have either $n_o \gg p_o$ or $p_o \gg n_o$, and the radiative lifetimes are for N-type material:

$$\tau_n' = 2\frac{p_o}{n_i}\tau_i = 2\frac{n_i}{n_o}\tau_i = \frac{p_o}{R_o} = \frac{1}{\gamma n_o} \tag{12}$$

for P-type material:

$$\tau_p' = 2 \frac{n_o}{n_i} \tau_i = 2 \frac{n_i}{p_o} \tau_i = \frac{n_o}{R_o} = \frac{1}{\gamma p_o} \qquad (13)$$

with the effective lifetime in intrinsic semiconductors given by

$$\tau_i = n_i / 2R_o \qquad (14)$$

the values of lifetime for the intrinsic material are clearly higher than those in extrinsic samples.

4) Semiconductors with High Excitation Level

For a high excitation level, $\Delta n \gg (n_o + p_o)$, and we obtain the following relationships

$$\Delta R = R_o (\Delta n)^2 / n_i^2 \qquad (15)$$

$$\tau_n = \tau_p = \frac{n_i^2}{R_o} \frac{1}{\Delta n} \qquad (16)$$

In this regime, we have quadratic recombination since ΔR depends on the square of the non-equilibrium density.

C) EVALUATION OF RECOMBINATION RATE

This framework of formulae offers useful guidance for the computation of recombination rates in a number of cases of interest. We shall now introduce the explicit expression for R_o, as suggested originally by van Roosbroeck and Shockley:

$$R_o = 32\pi^2 c\,(kT/ch)^4 \int_o^\infty \frac{n^3 K u^3\, du}{\exp(u) - 1} \tag{17}$$

$$= 1.785 \times 10^{22} (T/300)^4 \int_o^\infty \frac{n^3 K u^3\, du}{\exp(u) - 1} \left[\ cm^{-3}\, sec^{-1}\ \right]$$

Here $u = h\nu/kT$ is the integration variable, n is the refractive index and nK is the extinction coefficient.

Van Roosbroeck and Shockley integrated this expression by using experimental data on the optical parameters of Si and Ge obtained by H. B. Briggs[2]. The final relationship for the recombination rate at room temperature in high purity germanium is given as follows

$$R_o = 1.57 \times 10^{13}\ cm^{-3}\, sec^{-1} \tag{18}$$

Since the index of refraction and the extinction coefficient are

important parameters in these considerations, we have assembled these data from the published literature. In Figure 1, the refractive indices are given for germanium and silicon for the region between 1.0 and 3.0 μm. These results are derived mainly from the work by Briggs with additional points at the longer wavelengths abstracted from the studies of C. D. Salzberg and J. J. Villa[3] and of D. H. Rank, H. E. Bennett and D. C. Cronemeyer[4].

In Figure 2 the absorption coefficients of Si and Ge are given as a function of wavelength in the interval between 1.0 and 2.0 μm. These data are abstracted from the results by W. C. Dash and R. Newman[5]. For the sake of clear distinction, we should give the relationship between the absorption coefficient K plotted here and the extinction coefficient κ used in the formula by van Roosbroeck and Shockley

$$\kappa = \frac{K\lambda}{4\pi} \tag{19}$$

so that κ is dimensionless, as required.

The purpose of this evaluation is to obtain the integral and differential parameters for radiative recombination in the two materials of immediate interest to this program, namely germanium and silicon. Values for InSb will be reviewed also, since this material represents a rather opposite case

to that of Ge or Si because of its narrow forbidden band.

The integral values for R_o can be computed from the knowledge of the dispersion of the refractive index (Figure 1) and from the absorption coefficient (Figure 2), in addition to the evaluation of the universal function $u^3/\exp(u) - 1$, where $u = h\nu/kT$. The data by van Roosbroeck and Shockley and also those by E. Burstein and P. H. Egli[6] seem to point to the values listed below:

Material	ΔE (ev)	n_i (cm^{-3})	R_o ($cm^{-3} sec^{-1}$)	τ_i (sec)
Ge	0.7 ev	$2.4 \cdot 10^{13}$	$2 \cdot 10^{13}$	0.3
Si	1.1 ev	$1.4 \cdot 10^{10}$	$2 \cdot 10^{9}$	3.5
InSb	0.18 ev	$2.2 \cdot 10^{16}$	$2 \cdot 10^{22}$	$0.4 \cdot 10^{-6}$

For order of magnitude calculations of the radiation generated, we could use the above values for R_o. However, it is more illuminating to consider the differential rates per unit frequency or waveband interval. To secure this information we approach the problem in two ways. First, we obtain the differential spectrum just by folding the universal function into the dispersion and extinction for Ge. This relationship is given in Figure 3 over the wavelength range of interest.

The second method represents a useful approximation. We notice from Fig. 3 that the main contribution to the integral is due to the interval around the absorption edge where the absorption index is fairly low and the dispersion relatively small. We can therefore neglect the dispersion and adopt a constant refractive index. We then obtain a simpler expression for the recombination rate R_o

$$R_o = 4 n^2 \int_o^\infty KQ(\lambda)\, d\lambda \qquad (20)$$

where K is the absorption coefficient and $Q(\lambda)$ is the Planck function for surface emission

$$Q(\lambda) = 2 \pi c \lambda^{-4} / \left[\exp(h\nu / kT) - 1 \right] \qquad (21)$$

The equilibrium rate of photon generation per unit waveband and per unit volume is then simply

$$r_o = 4 n^2 KQ \qquad (22)$$

where the relationship between r_o and R_o is clearly

$$R_o = \int_o^\infty r_o\, d\lambda \qquad (23)$$

These formulae are of practical importance in the evaluation of the radiative output from selected semiconductor samples. At this point we can already forecast that the DR emitted from silicon devices will be significantly smaller than from germanium devices because of the appreciable differences in the forbidden gap and in R_o.

A further point to note concerns the temperature dependence of the emission. The temperature term appears both in front of the integral and in the exponential term of equation (17). The net effect is that R_o depends strongly on T. For a temperature increase from 300°K to 350°K, R_o increases from approximately 10^{13} to 10^{15} cm^{-3} sec^{-1}. Thus, a higher output yield could be expected at higher temperatures. However, we should examine also the competing thermal emission to decide if such mode of operation would be favorable for detection at a higher signal-to-noise level.

D) RADIATION FROM INDIRECT TRANSITIONS (TRAPPING CENTERS)

The radiation emitted from germanium and silicon samples has been investigated experimentally in the early fifties. Results on radiation from germanium are given briefly by J. R. Haynes and H. B. Briggs[7] and by Newman[8] and, later on, again by J. R. Haynes[9]. Data on radiation from silicon is reported by J. R. Haynes and W. C. Westphal[10].

The spectrum of the radiation emitted from germanium points to the existence of at least two distinct peaks, one occuring at 1.52 μm (0.81 ev) and the second at 1.75 μm (0.70 ev). The radiation appearing in the 1.52 μm region has been tentatively ascribed to direct transitions, whereas the second is attributed to indirect transitions involving phonon cooperation.

For silicon there are at least three maxima in the spectra. The peak at 1.13 μm (1.10 ev) has been related at least in parts to indirect intrinsic radiation. The other two peaks at 1.16 μm (1.072 ev) and at 1.195 μm (1.038 ev) are attributable to extrinsic radiation. The first transition appears to involve unionized boron atoms and the second arsenic atoms. No radiation due to direct intrinsic transitions was found in the spectrum.

The analytical description for this situation is rather difficult and requires the knowledge of a number of microscopic parameters. We can first assume that trapping centers act both on electrons from the conduction band and on holes from the valence band. The basic processes involved in recombination by trapping are therefore electron capture, electron emission, hole capture and hole emission.

The statistics of the recombination of holes and electrons has been treated by W. Shockley and W. T. Read[11]. The mathematical

formalism can be applied in the context of this problem. However, it is then difficult to extract precise numerical guidance because a number of microscopic parameters are not known even at this date.

We shall examine here only the case for nonequilibrium conditions in which electron and hole pairs are generated at some constant rate by carrier injection during operation of the device. Under steady-state conditions, the net rate of electron capture must be equal to that of the holes. The net recombination rate is then obtained in the following form

$$R = C_n C_p (pn - p_1 n_1)/\left[C_n (n + n_1) + C_p (p + p_1) \right] \qquad (24)$$

where the product $p_1 n_1$ is independent of the trap level E_t and is equal to

$$p_1 n_1 = N_c N_v \exp(E_v - E_c)/kT = N_c N_v \exp(-E_g/kT) = n_i^2 \qquad (25)$$

The following symbols apply

C_n = probability per unit time that conduction band electron will be captured by empty traps

C_p = probability per unit time that valence band hole will be captured by traps filled with electrons

n, p = density of electrons and holes in conduction and valence band, respectively

N_c, N_v = effective density of levels for conduction and valence band, respectively

E_c = energy of lowest conduction band level

E_v = energy of highest valence band level

E_g = energy gap = $E_c - E_v$

We should now examine also the problem of lifetime since we appreciate the importance of this parameter as an indication of the recombination rates. We shall distinguish here two basic situations. First, we shall express the case for a low disturbance in carrier density and then we shall treat the other extreme of a large disturbance.

1) Case of Low Carrier Density Injection

For the first case, adopting the terminology used in the previous chapter, we obtain the following expression for the lifetime

$$\tau = \tau_p^{\circ} (n_o + n_1 + \Delta n)/(n_o + p_o + \Delta n) + \tau_n^{\circ} (p_o + p_1 + \Delta n)/(n_o + p_o + \Delta n) \qquad (26)$$

Here n_o and p_o are the usual thermal equilibrium values of electron and hole densities. Furthermore, we define

$$\tau_p^\circ = 1/C_p \qquad \tau_n^\circ = 1/C_n \tag{27}$$

as the lifetime for holes in highly n-type material and the lifetime of electrons in highly p-type material.

For small values of Δn, the lifetime reduces to

$$\tau = \tau_p^\circ (n_o + n_1)/(n_o + p_o) + \tau_n^\circ (p_o + p_1)/(n_o + p_o) \tag{28}$$

2) Case of Large Carrier Density Injection

For the case of large injected carrier densities the expression for the lifetime is modified to

$$\tau = \tau_o \left\{1 + \Delta n (\tau_p^\circ + \tau_n^\circ)/\left[\tau_p^\circ (n_o + n_1) + \tau_n^\circ (p_o + p_1)\right]\right\} \cdot \left\{1 + \Delta n/(n_o + p_o)\right\} \tag{29}$$

Here τ_o is the lifetime for small Δn, as given by equation (28). The limiting value of τ as $\Delta n \to \infty$ is then simply

$$\tau_{\infty} = \tau_p^{\circ} + \tau_n^{\circ} \qquad (30)$$

These formulae offer some guidance for the evaluation of the radiative contribution via the carrier trapping mechanism. The outcome of this interaction can be either radiative output or phonon excitation.

E) IMPACT RECOMBINATION MECHANISM

During radiative recombination the laws of energy and momentum conservation are satisfied simultaneously in one of two ways. In the first case, the electron and hole have equal and opposite momenta and the emitted quantum has practically zero momentum but carries all the energy generated during recombination. In the second case, a third body is involved which can gain or lose momentum and thus enables electrons and holes of different momenta to recombine. A phonon could be assumed to play the role of the third body. In this case, any energy excess acquired (or lost) would then be equilibrated by collisions with the lattice. However, the energy evolved during recombination is on the order of the forbidden bandwidth of the semiconductor, that is 1 - 2 ev. This amount of energy is too large to be absorbed by a single phonon and a process involving the simultaneous participation of a number of phonons is not very probable. This difficulty is presently avoided by allowing the interaction

between carriers. In this case, the energy generated is transferred to a free carrier which gradually interacts with the lattice by collisions. This case, known as impact recombination or IR, applies both to DR and to TR and it involves three particles (two electrons and one hole or two holes and one electron).

The probability of triple collision of two electrons and a hole is proportional to n^2p and for two holes and an electron it is proportional to np^2. We can express therefore, the rate of change of electron and hole concentrations due to IR

$$\frac{dn}{dt} = \frac{dp}{dt} = -\eta_n n^2 p - \eta_p p^2 n \qquad (31)$$

where η_n and η_p are the impact recombination coefficients for energy transfer to an electron and to a hole, respectively.

1) <u>High Excitation Level</u>

For the case of high excitation level, defined by

$$\Delta n\ (\Delta p) \gg n_o + p_o \qquad (32)$$

we obtain for the rate of change

$$-\frac{d}{dt}\Delta n = \frac{d}{dt}\Delta p = \eta_n (\Delta n)^2 \Delta p + \eta_p (\Delta p)^2 \Delta n \qquad (33)$$

and for the lifetime

$$\tau = \frac{\Delta n}{\frac{d}{dt}\Delta n} = \frac{1}{(\eta_n + \eta_p)(\Delta n)^2} \qquad (34)$$

which indicates a strong quadratic dependence on carrier density.

2) Low Excitation Level

For a low excitation level, defined by

$$\Delta n\,(\Delta p) \ll n_o + p_o \qquad (35)$$

we find for the electron lifetime

$$\frac{1}{\tau_n} = -\frac{1}{\Delta n}\frac{d}{dt}\Delta n = \eta_p p_o^2 + 2\eta_n n_o p_o + \frac{\Delta p}{\Delta n}(\eta_n n_o^2 + 2\eta_p n_o p_o) \qquad (36)$$

and the hole lifetime is expressed by

$$\tau_p = \frac{\Delta p}{\Delta n} \tau_n \tag{37}$$

If $\Delta n = \Delta p$, then $\tau_n = \tau_p$. For the case of strongly n-type material $(n_o \gg p_o)$

$$\tau_n = \tau_p = \frac{1}{\eta_n n_o^2} \tag{38}$$

and for strongly p-type material $(p_o \gg n_o)$

$$\tau_n = \tau_p = \frac{1}{\eta_p p_o^2} \tag{39}$$

The recombination in this case depends strongly on the density of the majority carriers and collisions increase the rate of this event.

N. Sclar and E. Burstein[12] have attempted to derive an impact recombination coefficient based on the model of hydrogen-like impurity centers. The IR coefficients tabulated by these authors for Ge and Si are given as follows

	Ge n-type	Ge p-type	Si n-type	Si p-type
$B \cdot n$ ($\frac{cm^3}{sec}$) at 4.2°K	$3.5 \cdot 10^{-18} n$	$3.5 \cdot 10^{-18} n$	$2.9 \cdot 10^{-19} n$	$1.2 \cdot 10^{-19} n$
$B \cdot n$ ($\frac{cm^3}{sec}$) at 300°K	$0.6 \cdot 10^{-21} n$	$0.6 \cdot 10^{-21} n$	$0.5 \cdot 10^{-22} n$	$0.2 \cdot 10^{-22} n$

It should be noticed that the dimensions of the coefficients η given before are dimensionally equivalent to B. The evaluation of $B \cdot n$ for the 300°K point is extrapolated from the $1/T^2$ dependence given by Sclar and Burstein.

F) THERMAL RADIATION FROM SEMICONDUCTORS

We are interested here in computing the thermal emission to be expected from a semiconductor slab of refractive index n and of absorption constant K.

The volume rate of photon generation for unit waveband and in a small solid angle $d\omega$ is given straightforwardly from black body theory

$$r d\omega = n^2 K Q d\omega / \pi \tag{40}$$

where Q is the Planck function given by

$$Q = 2\pi c \lambda^{-4} / \left[\exp(h\nu/kT) - 1 \right] \text{ (photons/cm}^3 \cdot \text{sec)} \tag{41}$$

The total radiation reaching the upper surface of the slab may be found by integration over its thickness x

$$\int_0^x r \exp(-Kx)\, dx\, d\omega = r\left[1 - \exp(-Kx)\right] d\omega/K = n^2 Q\left[1 - \exp(-Kx)\right] d\omega/\pi \qquad (42)$$

We shall now use $t = \exp(-Kx)$ for the sample transmissivity and R for its reflectivity. Taking into account multiple internal reflections, we obtain then for the radiation emitted from the upper surface

$$\frac{r(1-t)(1-R)\,d\omega}{K(1-Rt)} = \frac{Q}{\pi}\,\frac{(1-R)(1-t)}{(1-Rt)}\,d\Omega \qquad (43)$$

here $d\Omega = n^2 d\omega$ is the solid angle into which the radiation is refracted. Since the normal blackbody photon emission is simply $(Q/\pi)d\Omega$, we can express the material emissivity in terms of R and t:

$$\epsilon = (1-R)(1-t)/(1-Rt) \qquad (44)$$

For a highly absorbing slab, we obtain

$$t \approx 0\ ;\ \epsilon \approx 1 - R \qquad (45)$$

For a highly transparent slab, on the other hand

$$t \to 1\ ;\ \epsilon \to 0 \qquad (46)$$

The emissivity of a semiconductor is therefore expected to

be fairly high at the short wavelengths and it should decrease sharply in the vicinity of the absorption edge. This effect has been indeed detected by Moss and Hawkins[13] for Ge and InSb.

There are a number of different processes which could lead to thermal emission from a semiconductor sample which is of interest here. The simplest mechanism is that due to periodic (we assume here that the excitation current through the sample will be pulsed and not DC) heating of the lattice by the transiently injected current carriers. This contribution may be evaluated by means of the preceding formulae by assuming the appropriate value of the temperature fluctuation.

A second effect is due to the change of the absorption coefficient upon carrier injection. Since this mechanism alters the transmitted and emitted radiation, the resultant effect is equivalent to a modulation of the previously defined emissivity ε. If we label the transmissivity in the presence of excess carriers $t_c = \exp(-K_c x)$, and neglecting changes in the reflectivity (changes of only a fraction of a percent have been reported by I. Filinski[14]), we obtain the following modulation function:

$$\Delta r d\omega = \left[\frac{t_c}{1 - Rt_c} - \frac{t}{1 - Rt}\right](1 - R^2)\, r d\omega + \left[\frac{1 - t_c}{1 - Rt_c} - \frac{1 - t}{1 - Rt}\right](1 - R)\, r_c d\omega \qquad (47)$$

where $r_c d\omega$ is the usual volume generation rate of photons at the higher temperature equivalent to carrier injection and $r d\omega$ is the volume generation rate of the quiescent background.

In the regime where the reflectivity is small and $t \gg 1$ (not too thin samples) so that we may neglect both quadratic and linear terms, we may use in first approximation simply

$$\Delta r d\omega \approx (t_c - t) r d\omega + (t - t_c) r_c d\omega \qquad (48)$$

The value of the transmissivity can be obtained from the knowledge of the absorption cross-section σ and of the carrier density n or p. For germanium, these data can be extracted from the work by Fan, Spitzer and Collins[15] for free carrier absorption and by Briggs and Fletcher[16] for hole absorption. The cross-section is a function of wavelength and sample temperature. For the region of initial interest in these studies (1 - 2 μm) the absorption coefficient for germanium may be approximated by

$$K_{Ge} \approx (10^{-17} n + 10^{-18} p)\ cm^{-1} \qquad (49)$$

Thus, t and t_c can be computed for each specific case and the modulation function can be evaluated. For the case of silicon, the experimental data

are abstracted from Spitzer and Fan[17] and for the same wavelength interval we obtain an absorption coefficient

$$K_{Si} \approx (10^{-17} n + 10^{-17} p)\ cm^{-1} \qquad (50)$$

which allows to compute the modulation expected in this material.

A final note of interest should be inserted here concerning the similarity between the spectral dependence of thermal radiation and recombination radiation. In effect, if we compare the thermal radiation reaching the upper surface of a slab of thickness x

$$\int_0^x r \exp(-Kx)dx\,d\omega = n^2 Q\left[1 - \exp(-Kx)\right]d\omega/\pi \qquad (51)$$

with the excess radiation rate Δr generated by injected carriers Δn and arriving under the same geometrical conditions

$$\int_0^x \Delta r \exp(-Kx)dx = 8n^2 Q\left[1 - \exp(-Kx)\right]\Delta n/n_i \qquad (52)$$

we notice that the spectral functions will be the same for equal temperatures. The only difference to be expected is in the lifetime of the decay for thermal relaxation of the lattice as compared with the recombination lifetime of free carriers.

III) RADIATIVE LOSSES DURING EMISSION

A) REFRACTIVE LOSSES

We are interested now in determining in some detail refractive and dispersive effects which the radiation emitted from the bulk of the semiconductor will suffer before leaving the sample.

First of all, we realize that the semiconductor materials of interest, mainly Ge and Si, possess a high index of refraction (see Fig. 1). In the wavelength region considered here, $n_{Ge} \approx 4.1$ and $n_{Si} \approx 3.5$. This implies that all the radiation observed externally with respect to the sample will have originated within a cone angle of 14°10' for Ge and 16°40' for Si; the axis of this cone is clearly the surface normal. Radiation impinging at larger angles against the internal sample surface will be totally reflected.

The internal reflection for normal incidence can be evaluated by the Fresnel formula

$$R = \frac{(n-1)^2 + K^2}{(n+1)^2 + K^2} \qquad (1)$$

Thus $R_{Ge} \approx 0.37$ and $R_{Si} \approx 0.31$, since for both materials $K^2 \ll 1$ for $\lambda > 1\ \mu m$. These values are in complete agreement with the reflectivity measurements by W. G. Spitzer and H. Y. Fan [18].

For other angles, the transmitted and reflected amplitudes are first evaluated by means of the Fresnel equations. The intensities are then obtained by squaring the amplitudes. We are interested particularly in the refracted amplitudes given by

$$\frac{E_s'}{E_s} = \frac{2 \sin \varphi \cos \varphi'}{\sin (\varphi + \varphi')} \qquad (2)$$

$$\frac{E_p'}{E_p} = \frac{2 \sin \varphi \cos \varphi'}{\sin (\varphi + \varphi') \cos (\varphi' - \varphi)} \qquad (3)$$

Here E and E' are the amplitudes of the electric field vector for the wave incident and refracted of vibration perpendicular ("s") and parallel ("p") to the plane of incidence. The angles φ and φ' are the corresponding angles of incidence and refraction from the dense medium (semiconductor sample) into the air. The internally reflected (R) and the refracted (R') percentage of the incident intensity are calculated here for a few angles of incidence

	Ge		Si	
	R	R'	R	R'
$\varphi = 0°$	37%	63%	31%	69%
$\varphi = 5°$	86%	14%	82%	18%
$\varphi = 10°$	91%	9%	86%	14%
$\varphi = 14°10'$	100%	0%	93%	7%
$\varphi = 16°40'$	100%	0%	100%	0%

These figures illustrate the well known fact that it is difficult to extract radiation from a semiconductor because of the large index of refraction of the medium. However, in view of the large maximum refracted angles, $\varphi'_{Ge} \approx 76°$ and $\varphi'_{Si} \approx 73°$, it appears advisable to use some light collecting system to minimize further coupling losses to the detector. This problem will be examined in connection with the detector input coupling requirements.

B) ABSORPTION LOSSES

The losses due to absorption must be compounded with the refractive losses to determine the net emission from the semiconductor sample. We have already shown that the total radiation reaching the two surfaces can be obtained by integration over the sample thickness ℓ

$$\int_0^{\ell} r\,(\exp - Kx)\,dx = r\,(1-T)/K \qquad (4)$$

where the transmissivity $T = \exp(-K\ell)$. Making allowance for multiple internal reflections and for superposition of upward and downward directions, we obtain for the radiation reaching the upper slab surface

$$r\,(1-T)/\left[K\,(1-RT)\right] \qquad (5)$$

Therefore, the total radiation emitted from the surface, accounting for the final refractive loss, obtains to

$$r' = \frac{r\,(1-T)\,(1-R)}{K\,(1-RT)} \qquad (6)$$

and in terms of the actual emission for recombination radiation

$$r' = \frac{8n^2\,Q\,(1-T)\,(1-R)}{(1-RT)}\,\frac{\Delta n}{n_i} \qquad (7)$$

The absorption coefficient K is given for both Ge and Si in Fig. 2 for the region between 1 and 2 μm. We can now evaluate the maximum value of the emission under assumption of normal incidence. For $K\ell = 1$, the emission for Ge is reduced to 0.46 and in Si to 0.49 from the previously presented figures. The contribution of all refractive angles is clearly a complex analytical problem suitable for treatment by electronic computer. This step is beyond the objectives of the present program.

IV) TRANSMISSION OF RADIATIVE SIGNAL

A problem of substantial practical importance during the conduct of forthcoming studies on radiation emitted by semiconductors concerns the transmission of such signal to a suitable detector.

The requirements imposed on the transmission line include low losses, wideband transfer characteristics and efficient coupling at the source and at the detector terminals.

The choice is here between propagation in a dielectric medium and propagation in a metallic pipeline, and these two methods shall be treated here in detail to analyze their applicability in the wavelength region of interest.

A) TRANSMISSION THROUGH DIELECTRIC MEDIUM

Total internal reflection in a dielectric medium can be used as a method for transmitting an available luminous signal over a required distance with low attenuation.[19]

For the purpose of collecting the radiation expected from a semiconductor slab, we are interested in evaluating acceptance angle, entrance and exit attenuation factors and attenuation along the lightguide. In addition, the spectrum transmission function should also be known. These factors will allow a precise evaluation of the output intensity for any given input signal.

First of all, we are interested in determining the numerical aperture of the lightguide

$$NA = \sin\theta = \sqrt{n_1^2 - n_2^2} \qquad (1)$$

The half angle θ describes maximum incidence for a transmitted ray. This angle is related to the index of refraction n_1 of the fiber core and to that of the outer cladding n_2, for total internal reflection $n_1 > n_2$.

For the fibers available for this program, the entrance angle (half angle) ranges from 30° to 39° corresponding to a NA = 0.5 → 0.63. The index of refraction of the core is generally n_1 = 1.62 and that of the cladding n_2 = 1.49 → 1.54.

Second, we shall evaluate the losses at the entrance aperture due to Fresnel reflection

$$R_F = \left(\frac{n_1 - 1}{n_1 + 1}\right)^2 \qquad (2)$$

In this case, for perpendicular incidence and for a smooth entrance surface, we obtain R_F = 0.056 for n_1 = 1.62. Thus, the entrance losses are approximately 6%. For the exit aperture the losses are the same since the Fresnel formula is modified to

$$R_F = \left(\frac{1 - n_1}{1 + n_1}\right)^2 \qquad (3)$$

We evaluate next the transmission losses expected for the spectrum range of interest. In Figs. 4 and 5, we present the transmission for typical glass and plastic fibers. From these data, we can now infer an average attenuation coefficient for the region between 1 and 2 μm for which emission is anticipated. For any luminous input signal I_o, the output available after transmission through a length ℓ will be approximately

$$I = I_o \exp(-\alpha\ell) \qquad (4)$$

From the data of Fig. 5, we shall assume a conservative figure of 60% for the transmission over one foot length. Therefore, the attenuation coefficient will be $\alpha \approx 0.3/\text{ft}$.

Finally, the total transmission, including Fresnel losses at the entrance and exit apertures, will be about

$$T = (1 - R_F)^2 \exp(-\alpha\ell) \qquad (5)$$

For the practical case of interest here $R_F = 0.06$ and $\ell = 1.5$ ft., thus $T \lesssim 57\%$.

B) TRANSMISSION THROUGH LIGHTGUIDES

Lightguides are essentially greatly oversized waveguides which are used without mode discrimination, thus the transmission occurs in many very high order modes. The transmission is more

easily described in terms of geometrical optics by following the multiple reflections which a plane wave undergoes when passing through the pipe.

The adoption of this type of hardware is common practice for far-infrared applications. We intend to examine here the possibility to extend this use to the near infrared to obtain a wide passband for the radiation of interest (thermal and non-thermal).

The reflection coefficient of a metallic conductor can easily be computed by means of electromagnetic theory[20]. The expressions used here apply strictly for very high reflectivity (close to one), which is the case for practically all metals for wavelengths of 10 μm or longer. For smaller wavelengths, the differences become progressively more appreciable and, finally, for the visible range, the macroscopic electromagnetic theory is no longer applicable. For the intermediate region of interest here the results are expected to have still some validity, particularly if metals are selected which exhibit still very high reflectivities to as short a wavelength as 1 μm (e.g., Ag, Au, Cu).

The reflection coefficient can be given for polarization perpendicular (R_s) and parallel (R_p) to the plane of incidence

$$R_s \approx 1 - 2x\alpha \qquad (6)$$

$$R_p \approx \frac{2\alpha^2 - 2x\alpha + x^2}{2\alpha^2 + 2x\alpha + x^2} \qquad (7)$$

where α is the grazing angle and x is given by

$$x = 0.18\,(\rho/\lambda)^{\frac{1}{2}} \qquad (8)$$

When the number of reflections N is large, it can be shown that both polarizations are attenuated exponentially down the light guide with the parallel polarization more rapidly attenuated than the perpendicular. The total transmission is then found by integration over the solid angle of the incoming radiation and can be computed from

$$T = \tfrac{1}{2}\exp(-2q) + \left[1 - \exp(-q/2F^2)\right]F^2/q$$

$$\approx \tfrac{1}{2}\left[1 + \exp(-2q)\right] - q/8F^2 \qquad (9)$$

where $q = x\,(L/d) = 0.18\,(\rho/\lambda)^{\frac{1}{2}}(L/d)$

Here, ρ = resistivity of the metal wall in Ωcm,

λ = wavelength of radiation in cm

L = length of the pipe of diameter d

F = f/number of incoming radiation

We obtain now for a gold plated conductor with a thickness of several skin depths

$$T \approx \tfrac{1}{2}\left[1 + \exp\left(-\frac{0.057}{\lambda_{\mu m}^{\frac{1}{2}}}\,\frac{L}{d}\right)\right] - \left(\frac{0.028}{\lambda_{\mu m}^{\frac{1}{2}}}\,\frac{L}{8dF^2}\right) \qquad (10)$$

We compute the following table for transmission over the wavelength range of interest

	L/d → 100	10
λ		
10 μm	0.48	0.90
5 μm	0.44	0.88
2 μm	0.41	0.82
1 μm	0.40	0.77

We thus conclude that transmission in the medium and near infrared is still acceptable for present purposes. However, in order to retain reasonable values of transmission the ratio of L/d should not greatly exceed 100. Thus, we have to resort to very short distances between radiant source and detector. The diameter d should not exceed greatly the characteristic size of the object, otherwise the signal will be masked by the contribution of the background radiation.

V) EVALUATION OF RADIATION DETECTION PROBLEMS

We are interested here in evaluating the radiation emission expected from a generalized semiconductor geometry in order to assess the voltage signal and the signal-to-noise level to be encountered. This analysis will offer the necessary guidelines for the optimum detector type and geometry to be used. It will serve also in the selection of the electronic circuitry required to process the detected signal.

We shall first consider the response of the detector to an incoming radiant flux. Assuming operation in the photoconductive mode, the voltage V_s induced as a signal is caused by an increase Δn of the free carriers n normally present in the crystal

$$V_s = \frac{E}{(R_x + R_\ell)} \frac{R_x R_\ell}{(R_x + R_\ell)} \frac{\Delta n}{n} \qquad (1)$$

Here R_x is the crystal resistance, R_ℓ is the load resistance and E is the voltage provided by the bias battery.

For a detector crystal of area A, operating at a photoconversion efficiency e (radiant flux into free carriers) and with a carrier lifetime τ, the change in charge carriers Δn can be related to the incident photon flux Φ_s, thus transforming equation (1) into

$$V_s = \frac{E R_x R_\ell}{(R_x + R_\ell)^2} \frac{\epsilon \Phi_s A \tau}{n} \tag{2}$$

Φ_s comprises the photon flux up to the long wavelength cut-off of the detector.

For a time-varying generation of the radiant signal, the expression should be further modified to include the term

$$V_s' = V_s \frac{1}{(1 + \omega^2 \tau^2)^{\frac{1}{2}}} \tag{3}$$

We should now turn our attention to the noise expected from the detector element.

The Johnson noise can be evaluated from

$$V_{nj} = (4kTR_x)^{\frac{1}{2}} \tag{4}$$

where k is the Boltzmann constant and T is the temperature of the detector element. For a $1 M\Omega$ element at room temperature this is typically 10^{-7} v/$\sqrt{\text{Hz}}$ and at 4.2°K this reduces to about 10^{-8} v/$\sqrt{\text{Hz}}$. Thus, this source of noise is usually small compared to other types.

The 1/f noise should not be appreciable for frequencies above 100 Hz. This contribution was investigated by A. V. MacRae and H. Levinstein[21] who suggest the following relationship for the noise voltage:

$$V_{n,f} = 2\sqrt{B(I^2 R_x / f)} \tag{5}$$

where B is an experimentally determined constant and I is the current through the sample $= E/(R_x + R_\ell)$.

A major noise contribution is given by the generation and recombination (G-R) rates of the charge carriers. This problem has been examined by K. M. van Vliet[22] who proposed the following expression for the G-R noise

$$V_{n,gr} = 2 \frac{E R_x R_\ell}{(R_x + R_\ell)^2} \left(\frac{\tau \Delta f}{<\Delta n^2>} \right)^{\frac{1}{2}} \frac{1}{(1 + \omega^2 \tau^2)^{\frac{1}{2}}} \tag{6}$$

Here, $<\Delta n^2>$ is the variance in n and Δf is the amplifier bandwidth used. If the carriers are generated thermally by lattice vibrations, we have the case of G-R noise and $<\Delta n^2> = n$. On the other hand, if the background radiation dominates carrier production, we have photon noise (PN) and

$$<\Delta n^2> = \sum_\lambda n_\lambda \left(1 + \frac{1}{\exp(hc/\lambda kT) - 1} \right) \tag{7}$$

However, for $T_B = 300°K$ and $\lambda \leq 10\,\mu m$, the second term inside the parenthesis of equation (7) is always small, and $<\Delta n^2> \rightarrow n$ as for the GR noise.

The performance of the detector is conveniently expressed in terms of the detectivity which relates the signal-to-noise ratio to the incoming rms power

density P_s. The normalized detectivity D* is generally adopted in order to define a parameter which is independent of detector area.

$$D^* = \frac{V_s}{V_n} \frac{(\Delta f)^{\frac{1}{2}}}{P_s A^{\frac{1}{2}}} \quad \text{cm Hz}^{\frac{1}{2}}/\text{watt} \tag{8}$$

This figure of merit defines the rms signal-to-voltage ratio obtained per watt of radiant power. Alternatively, the noise equivalent power NEP is obtained from

$$\text{NEP} = \frac{A^{\frac{1}{2}}}{D^*} = \frac{V_n}{V_s} \frac{AP_s}{(\Delta f)^{\frac{1}{2}}} \quad \text{watt}/\text{Hz}^{\frac{1}{2}} \tag{9}$$

and this parameter indicates the power required to obtain a signal-to-noise ratio equal to unity.

In terms of the previously used parameters, D* may be given as

$$D^* = \tfrac{1}{2} e A \left(\frac{\tau}{n}\right)^{\frac{1}{2}} \frac{\Phi_s}{P_s} \tag{10}$$

We shall now proceed with an estimate of the expected signal. First we consider the background emission due to temperature increase of the semiconductor slab. The assumption is made that the room temperature contribution can be masked by appropriate reduction of the field of view. The temperature of the substrate is estimated at 320°K under transient conditions during pulsing. This

would entail the following parameters:

T_b = 320°K

λ_{max} = 9 μm

W = $6 \cdot 10^{-2}$ watt/cm^2 (for emissivity = 1)

W_λ = $4.5 \cdot 10^{-3}$ watt/cm^2 · μm (at λ_{max})

Φ = $5 \cdot 10^{18}$ photons/cm^2 · sec

E_{max} = 0.14 ev (photon energy at λ_{max})

$W_{4\,\mu m}$ = 10^{-1} (fraction of energy radiated at 4μm)

$W_{2\,\mu m}$ = $6 \cdot 10^{-5}$ (fraction of energy radiated at 2μm)

If the thermal emission is detected against a background of appreciably lower temperature, or if the acceptance angle is sufficiently small, we estimate a signal at λ = 2μm of about 100μv. This evaluation entails an acceptance area of $2 \cdot 10^{-2}$ cm^2 (corresponding to a fiber lightguide of 0.030 inch diameter), a conversion efficiency of 10% and a detector responsivity of 10^6 v/w, which is typical for PbS at 77°K.

An accurate evaluation of the non-thermal radiation is not simple because it is predominantly trap radiation which is generated. However, we can obtain simple guidelines by using for ΔR the equations for the case of high excitation level. We obtain then

$$R = R_o + \Delta R = R_o \left(1 + (\Delta n)^2/n_i^2\right) \qquad (11)$$

Assuming an arbitrary injection such that $\Delta n = 2n_i$, R results to be $8 \cdot 10^{13}$ / cm^3 sec. If the average photon energy is 1 ev and the conversion efficiency is 10^{-4}, we expect a power of 10^{-9} watt or a signal of 10^{-3} volt at a responsivity of 10^6 volt/watt. This value is however an upper bound. For the more realistic case of a low excitation level, the signal should be reduced by at least one order of magnitude.

Thus, the non-thermal radiation may well be of the same order of magnitude as the thermal radiation emitted in the same waveband. The only discrimination possible is by means of the characteristic decay time after carrier injection; for the non-thermal emission the recombination times are rapid, at least in heavily doped semiconductors, whereas the decay of the lattice temperature is a slow process governed by thermal diffusion.

VI) DISCUSSION OF EXPERIMENTAL EFFORT

In the late forties, a number of reflecting and reflecting-refracting microscopes were developed, suitable for scanning objects in the near-infrared range [23,24,25,26]. The use of these instruments in determining temperature profiles in microstructures is therefore reasonably old and several combinations of microscopes and radiometers have been described in the literature [27,28]. The use of fiber optics eliminates the requirement for a collecting reflective system, although it limits the response to the passband available at this time in commercial fibers, which is approximately to 2 μm. Thus, the transmission of room temperature radiation is severely attenuated. In the future, with the possible development of glass fibers of wider passband this drawback may be remedied.

In view of this situation, the basic objective of the brief experimental effort conducted during the course of this program is to attempt to determine the radiative mechanism of the emission from semiconductors. From the analysis of the results from tests carried out on several configurations, guidelines will be evolved for the adoption of the method in the diagnostic of operating solid state devices.

At the beginning of the experiments it was realized by means of theoretical evaluation that the signal of interest is a low intensity effect. Hence, main emphasis was given to high sensitivity of the detector and to minimizing radiative background and spurious electromagnetic interference. Initially, two detector configurations were considered. The first geometry is presented in Figure 6.

A liquid helium detector dewar (ADKIN Model RC-4) has been modified to provide a bottom-looking entrance aperture. This window features means for bringing a fiber lightguide of 0.032 inch diameter into the field of view of the cryogenic detector. A cryogenically-cooled lightguide is used for high efficiency coupling and to decrease the radiative background noise. A simple change of entrance plate allows to reduce the size of the dielectric lightguide, if the detected intensity is sufficient. With this configuration, in combination with absorption filters, the radiative emission can be studued from simple semiconductor geometries which are amenable to analytical interpretation.

The second configuration is presented in Figure 7. The same cryogenic container is used. However, in this case, the dielectric entrance lightguide is replaced by a short metallic lightguide which is terminated with a dual detector system. One detector is designed for peak detectivity in the region of 8 - 10 μm, corresponding to black body emission at $T \approx 300°$ to 350°K. The second detector on the other hand, is peaked for detectivity in the near-infrared between 1 and 3 μm. In this fashion, we hoped to be able to correlate the radiative emission from direct or indirect transitions with thermal emission due to phonon excitation. The operation is planned first for the kHz frequency region. This allows the use of low-noise preamplifiers (ADKIN Type F-60) with only 10 nv/$\sqrt{\text{Hz}}$ noise.

The semiconductor test samples are installed on a N/C two-axes precision

stage. The motion is programmable or manually selected. The displacement accuracy is 0.00003 inch, which is ample for the scanning resolution required for this study.

Appropriate electronic circuits are used to pulse modulate the semiconductor devices with selected time cycles. The behavior of the device is studied simultaneously on an oscilloscope curve tracer, Tektronix model 576.

VII) CALIBRATION OF INFRARED DETECTORS

The detectors selected for studying the radiation emitted from the semiconductors are photoconductors of the PbS and GeHg type. Detection can be carried out with the PbS in the band between 1 and 4 μm and with the GeHg detector between 2 and 15 μm. The first detector has maximum responsivity at 3.5 μm and the second at approximately 10 μm. It is therefore possible in principle to detect predominantly thermal radiation and to discriminate the same from possible recombination radiation emission.

The first step during the experiments was to calibrate carefully these detectors to determine the characteristic parameters and to insure that they are suitable for the detection of the feeble radiation anticipated here.

The PbS detector is designed to operate at approximately 77°K and the GeHg at 4.2°K. Since they are connected to the same cryogenic reservoir, runs were taken at both temperatures to determine the response.

The experimental set-up consisted of the following equipment:

i)	Adkin BB-500	Blackbody Vacuum Source
ii)	Adkin VSM-1	Chopper and Filter Assembly in Vacuum Housing
iii)	Adkin RC-4-A	Research Dewar
iv)	Adkin F-60-2	60 db Gain Low Noise Preamplifier
v)	Krohn-Hite 3103	Variable Filter
vi)	Princeton Applied Research Model 121	Lock-in Voltmeter

The experimental set-up was the following: the temperature of the black body calibration source was selected to be 500°K and was maintained to a precision of better that 1°K by means of an electronic control and sensing circuit. The emitted power is lightpiped by means of precision lightguides in the vacuo to a chopper and filter housing. This allows to modulate and to filter the radiation to study the response at a few wavebands. The modulated radiation is lightpiped finally into the low temperature dewar. Biasing currents for the detectors is provided by low noise triaxial networks and the signal is fed to the lock-in voltmeter via a very low noise preamplifier. The solid angle of the detector system is defined by an aperture stop in a vapor-cooled radiation shield and by the acceptance angle of the condensing cone. To eliminate absorption effects, all the measurements were conducted under evacuated conditions.

From the temperature and the emissivity of the blackbody and from the computed attenuation, we infer the radiant energy impinging on the detector elements. Response and noise are then related to the input power at several bias currents and for operating temperatures of 77° and 4°K. The results obtained from these calibration runs are presented in the following tables in terms of responsivity R (volt/watt), NEP (watt), NEP (watt/$\sqrt{Hz}$), D* (cm/Hz/watt).

VIII) EXPERIMENTS ON RADIATION FROM SEMICONDUCTORS

A) EXPERIMENTS WITHOUT SCREENING CAGE

The experimental effort is directed at obtaining some indication of the radiation emitted from simple simiconductor structures and at determining the functional dependence on carrier injection parameters.

The first series of tests entailed using transistor configurations in which the junction is exposed so that the emitted radiation can be detected without obstructions. This proved to be a problem because, in general, accessibility to any device is restricted due to the electrode configuration. A number of power transistors were opened in this attempt. Finally, we settled for a 2N1183 NPN power transistor which features a reasonably satisfactory geometry.

A pulser is used to produce an adjustable function (square wave, sinusoidal or triangular). The frequency of this output can be selected and the pulse is applied to program a Tektronix 576 curve tracer oscilloscope. The modulation function is therefore immediately visible on the screen together with the parameters of applied current and voltage.

In the initial tests, a single channel detector configuration was used (Figure 6) consisting of a high sensitivity calibrated PbS cooled to 77°K and with the output fed via an ADKIN low noise preamplifier model F-60-2 to a dual

channel CRO. The experiments were conducted in the open laboratory area without taking any particular shielding precautions. When the transistor is pulsed with a square wave function of 1 - 2 amps, a signal could be detected at the 200 μv level. A typical oscillogram is given in Figure 8 where two traces are synchronized relating the radiation signal to the modulation function. The time scale is 5 msec/cm corresponding to a repetition rate of 100 pps. The amplitude is 1 amp/cm. The signal from the detector is seen to increase almost linearly as a function of time after an initial transient due to the application of the current. Similarly, the signal decays after the pulse is turned off. The signal was determined to originate from the junction area since slight lateral motion by means of the numerically controlled stage causes an appreciable reduction in the intensity. There is some slight indication of the presence of two decay times, one in the sub-millisecond region and the second on the order of several milliseconds. The RC decay time of the detector circuit is estimated at about 100 μsec.

The next measurement entailed the detection of the signal level obtainable as a function of the base current through the transistor. The transistor was pulsed at variable repetition rates from 25 to 250 pps with a square wave up to 2.6 amp. The results obtained are given in Figure 9. The signals are seen to disappear when metallic or dielectric absorbing

materials are interposed in the light path.

A Waveform Eductor manufactured by PAR was also operated in these experiments. However, the results were unsatisfactory because the drift of the baseline makes the instrument rather useless for signal levels below 500 μv, and this is the upper bound of the region of interest here.

B) EXPERIMENTS INSIDE FARADAY SCREEN CAGE

A second phase of the experimental effort was aimed at the reduction of any spurious pick-up noise in order to improve the quality of the signal detected. The complete experimental system was set up inside a Faraday screen cage provided with floating power and line filters. The only portion of the equipment which was left outside and adjacent to the cage is the electronic circuitry for the drive of the numerically controlled stage. Screening cones were manufactured to surround the radiating semiconductor device and to prevent pick-up from the pulse generating equipment. This was a particularly time-consuming prodecure which required complete triaxial ducting of the signal. After careful elimination of other noise sources, significant signals could be detected down to a level of 10 nano-volt. Without similar extensive precautions it would be difficult to assess the validity of detected radiation signals.

A schematic drawing of the system installed in the Faraday cage is given

in Figure 10. Additional electronic components, e.g., oscilloscopes and others, are not shown. Lock-in preamplifiers (PAR Model 121 or HR8) are used with a low-noise preamplification stage (ADKIN F-60-2). The use of a waveform eductor is excluded at the low signal input voltages for the reasons discussed before.

The emission from a power transistor was investigated first. The transistor was the NPN type 2N1701 whose configuration is reproduced in Figure 11a and 11b. The fiber lightguide used has a diameter of 0.031 inch and a calculated acceptance half angle of 35°. Hence the resolution is not very good but acceptable for present purposes. The trace obtained from a scan across the configuration is given in Figure 12. In this case the stage was driven incrementally manually. After some readjustment of the scanning line, a slightly higher signal profile was obtained. At this point, the numerically controlled stage was activated and the output from the lock-in electronics was displayed on a recorder. The profile is presented in Figure 13. Full-scale deflection corresponds here to 5 μv, thus, the maximum amplitude is approximately 2.6 μv. The scanning line for this automatic display is given in Figure 11b. It is inferred from these results that the main portion of the radiation is detected across the emitter-to-base junction. The base-to-collector is unfortunately not accessible

in this configuration and in similar ones for reasons of thermal efficiency. Thus, the amplitude of the signal is certainly lower than that expected across the collector-to-base junction.

A test was therefore conducted to determine the possibility of obtaining increased signal by letting the fiberoptic lightguide look at an inclined angle with respect to the normal. By proper aiming, it should be possible to detect some contribution from the base-to-collector region since the configuration of the 2N1701 appears to have a mesa-like structure. The results of this test are given in Figure 14. It is evident that with increasing inclination (angle with respect to the normal) the detected radiation signal also incfeases.

The next test conducted was aimed at determining the radiative emission versus collector current and voltage. The results are plotted in Figures 15 and 16. For low values of V_{CE} up to 6 volts, the radiation signal appears to be nearly linear with current up to approximately 2.5 amp. At V_{CE} in excess of 10 volts, the relationship is non-linear and the radiation signal increases more rapidly with current.

A number of other transistor devices have been investigated. Among these are the following: RCA 40314, 2N696 (Si NPN), TR 02C. In most cases, the junction geometry could not be used for experimentation because the area of interest was obscured by electrodes or other material. The

signals amounted at best to 20-50 nv, and hence it was not possible to collect a clean set of data as in the case of the 2N1701.

A number of diodes were studied without detection of any appreciable signal. The highest current ratings were applied to the GE type 1N-2156R at 25 amp continuous duty and 400 amp surge. Observation was attempted laterally because of the inherent geometrical difficulties posed by nearly all diodes. The results were negative.

Gated bidirectional thyristors were also investigated because of the ability of conducting considerable current loads. The RCA model 40430 (Triac) yielded detectable signals at the level of several microvolts. Typical dependence of the radiative output on current amplitude is given in Figure 17. A momentary overload point is also entered to indicate that the radiation decreases appreciably under such conditions. The data were taken with the device operating at 120 Hz. A decrease in frequency to 60 Hz under equal current loading increased the signal by more than a factor of two (e.g. at 5 amp, V_s = 4.3 μv at 120 Hz and 11 μv at 60 Hz).

The operation with IC's was not particularly successful. A number of different configurations were investigated in detail but in every case the signals were too close to the noise level to be convincing. The maximum current injected was 50 ma into a 200 ohm load by using a Fairchild U5B-770939X operational amplifier which yielded an indication close to the noise level (10 nv).

IX) CONCLUSIONS AND RECOMMENDATIONS

The results obtained during the course of this program covering theoretical and experimental work on the detection of infrared radiation from semiconductors may be summarized as follows:

i) Signals attributable to radiative emission in the near-infrared have been detected from a number of semiconductor devices during operation. The maximum signal levels obtained with a cooled PbS detector with a responsivity of over 10^6 v/w amount to 10^{-4} v. In general, for most of the devices investigated, signals were acquired below the μv level.

ii) The small signals available impose extreme care in the experimental detection procedures adopted. The lightguide itself can give rise to the transmission of spurious signals from the pulsed circuitry which travel to the detector in form of dielectric waveguide perturbations. The disappearance of the signal when interposing a metallic boundary is not sufficient indication for the authenticity of the detected amplitude. Attention is drawn to the fact that the pulsed semiconductor becomes a radiating electromagnetic source which must be screened from the susceptible high-impedance detector. Thus, signals in excess of 10^{-4} v must be examined with particular care.

iii) Discrimination of the signals attributable to thermal as opposed to

non-thermal (DR, TR, IR) radiation has proved a difficult task. First of all, insertion of bandpass filters constitutes a sufficiently severe loss, so that usually the signal is reduced to the background level. This is due not only to the Fresnel losses at the filter interface, but even more so, to the rapid decrease in signal amplitude when the lightguide is removed from the immediate vicinity of the semiconductor surface. The experiments aimed at obtaining simultaneous signals at two wavelengths were not successful, since in this case the higher coupling losses due to metallic lightguide and separation of objects and detectors from the same reduced the signal to the nanovolt level. In general, we are inclined to believe that both components are always present in different proportions. In the operating mode where thermal effects are small, that is, for short pulse times, small current amplitudes and low repetition rates, the signal is probably mainly of non-thermal nature and is ascribable to recombination radiation due to the trap mechansim. In this regime, the radiation signal increases linearly with injection current, corresponding to the theoretical case of low carrier density injection. For higher currents and duty cycles, the signal is seen to increase at times nearly quadratically with injection parameters. This matches the expected behavior not only for high density injection but also for the appearance of thermal emission. This contribution depends greatly on the thermal dissipation in the device and the heat

conductivity to the attached heat sinks.

iv) The same argument can be drawn from the observation of decay times of the radiative signal. We characterize the decay of any thermal contribution by the diffusivity of heat in the semiconductor. From two-dimensional diffusion equations we can define a thermal diffusion time τ during which the heat stored in a given volume will be carried a distance ℓ

$$\tau = \ell^2 \rho c / \pi K \tag{1}$$

Here ρ is the density of the material, c is the specific heat and K is the thermal conductivity. For germanium and silicon, for instance, we obtain

$$\begin{aligned} \tau_{Ge} &= 0.858\, \ell^2 \\ \tau_{Si} &= 0.349\, \ell^2 \end{aligned} \tag{2}$$

Thus, for $\ell = 0.1$ cm, $\tau_{Ge} \approx 8.6$ msec, $\tau_{Si} \approx 3.5$ msec. This figure is well in line with signal decay as presented in Figure 8 which can be explained in terms of thermal diffusion times. On the other hand, the more rapidly decaying component (about 400 μsec), discernible after the turn-off of carrier injection, is attributable to decay by recombination

radiation. In this specific case, the contribution due to RR is clearly only about 20% of the total signal detected.

A further evidence of thermal contribution to the signal is seen under conditions when the injection current is maintained constant and the duty cycle is increased by prolonging pulse duration or repetition rate. This change always induces an increase of signal which can be interpreted in terms of additional thermal dissipation in the device.

v) The scanning of an appreciable number of devices across the junction region has always resulted in well defined profiles of the emitted radiation. In most of the cases studied, the peak resulted to be less than 0.010 inch or 250 μm in width, a figure which is set more by the finite aperture of the lightguide used (0.030 inch diameter) than by the inherent size of the radiating zone. Under cw application of power to the device, it would be difficult to explain the sharpness of the profile detected purely in terms of thermal radiation. These results, however, provide further evidence of simultaneous contribution of thermal and non-thermal radiation when the profile of the emission is examined in regions sufficiently remote from the junction to allow for decay and recombination of the injected carriers.

The above conclusions and comments pertain to the interpretation of the results gathered during these studies. We should now present some comments and

recommendations regarding the applicability of this method as a diagnostic tool in semiconductor technology.

i) In general, none of the configurations studied yielded any radiation through the original encapsulation material. For a metallic boundary this is obvious. However, for a dielectric encapsulation, thermal radiation can still be transmitted with attenaution. Thus, the method requires the availability of a device from which the encapsulation is completely removed or which is tested on the assembly line before the encapsulation stage is reached.

ii) It is difficult to detect the signal without a prior study of device configuration. Even with this knowledge, considerable difficulties are encountered in the detection because of configuration. In a number of instances, the areas of interest are completely or partially obstructed by electrode configuration or by solder or other material deposited during the encapsulation procedure. However, once the radiation from a given device is detected, it appears to be straightforward to extend the observation to any number of similar devices.

iii) During this study, little or no success was scored with low power devices, such as small diodes, low power IC's and similar. The signal in these cases is estimated to be less than 20 nv. On the other hand, the signal

levels from medium and high current transistors, triacs, SCR's and similar devices were sufficiently high for detection well above the noise and for acquiring sharp radiation profiles.

iv) The outlook for appreciable improvement in the amplitude of the detected signal is not particularly favorable. The PbS detector used here exhibits optimum parameters for detection of radiation in the 1 - 2 μm region. Avalanche detectors recently becoming available commercially have better time response but feature also relatively lower sensitivities and higher noise levels. For the detection of the thermal component, the use of fibers transmitting in the 5 μm wavelength will certainly increase the detection level.

v) The usefulness of infrared radiation detection in the study of operating microstructures is beyond doubt. Direction of future research and development efforts should be along the improvement of detector systems for acquisition of thermal radiation. The main emphasis here should be on fibers transmitting possibly all the way out to 10 μm. Materials with these properties have been available for a number of years. Therefore the practical realization of such fibers is just a development problem.

The question is now whether the additional detection of recombination radiation can contribute appreciably as a diagnostic tool. The method

could offer an indication of carrier density distribution in a given semiconductor. Thus, if the nominal values of n and p are known and Δn or Δp are measured, substantial information could be derived about the distribution of n and p in any accessible geometry and about the carrier decay with distance.

This adds appreciably to the knowledge of microconduction effects in the bulk of the material, hence as a diagnostic tool the RR method provides a more basic understanding than that afforded by the thermal radiation method alone. However, the RR detection method is presently beset by experimental difficulties which require experienced personnel to derive significant data and it is not readily suitable to assembly line production control.

The basic foundations for this method are now well established and its limitations are understood both theoretically and from the practical viewpoint of the experimentalist. In all those cases where the answers to be provided by the weak signal available from carrier recombination effects is worth the effort, its application is both feasible and recommended.

X) REFERENCES

1) W. van Roosbroeck and W. Shockley, Phys. Rev. 94, 1558 (1954)

2) H. B. Briggs, Phys. Rev 77, 287 (1950)

3) C. D. Salzberg and J. J. Villa, J. O. S. A. 47, 244 (1957)

4) D. H. Rauk, H. E. Bennett, D. C. Cronemeyer, J. O. S. A. 44, 13 (1954)

5) W. C. Dash and R. Newman, Phys. Rev. 99, 1151 (1955)

6) E. Burstein and P. H. Egli, Advances in Electronics, Volume VII, p. 56 (Academic Press, 1955)

7) J. R. Haynes and H. B. Briggs, Phys. Rev. 86, 647 (1952)

8) R. Newman, Phys. Rev. 91, 1313 (1953)

9) J. R. Haynes, Phys. Rev. 98, 1866 (1955)

10) J. R. Haynes and W. C. Westphal, Phys. Rev. 101, 1616 (1956)

11) W. Shockley and W. T. Read, Phys. Rev. 87, 835 (1952)

12) N. Sclar and E. Burstein, Phys. Rev. 98, 1757 (1955)

13) T. S. Moss and T. D. H. Hawkins, Proc. Phys. Soc. 72, 270 (1958)

14) I. Filinsky, Phys. Rev. 107, 1193 (1957)

15) H. Y. Fan, W. G. Spitzer, R. J. Collins, Phys. Rev. 101, 566 (1956)

16) H. B. Briggs and R. C. Fletcher, Phys. Rev. 91, 1342 (1953)

17) W. G. Spitzer and H. Y. Fan, Phys. Rev. 108, 268 (1957)

18) W. G. Spitzer and H. Y. Fan, Phys. Rev 106, 882 (1957)

19) R. N. Thorn and R. W. Waniek, Rev. Sci. Instr. 24, 391 (1953)

20) J. A. Stratton, Electromagnetic Theory (McGraw Hill Inc., 1941)

21) A. V. MacRae and H. Levinstein, Phys. Rev. 119, 62 (1960)

22) K. M. Van Vliet, Proc. IRE 46, 1004 (1958)

23) C. R. Burch, Proc. Phys. Soc., London, 59, 41 (1947)

24) B. K. Johnson, Jour. Sc. Instr. 26, 148 (1949)

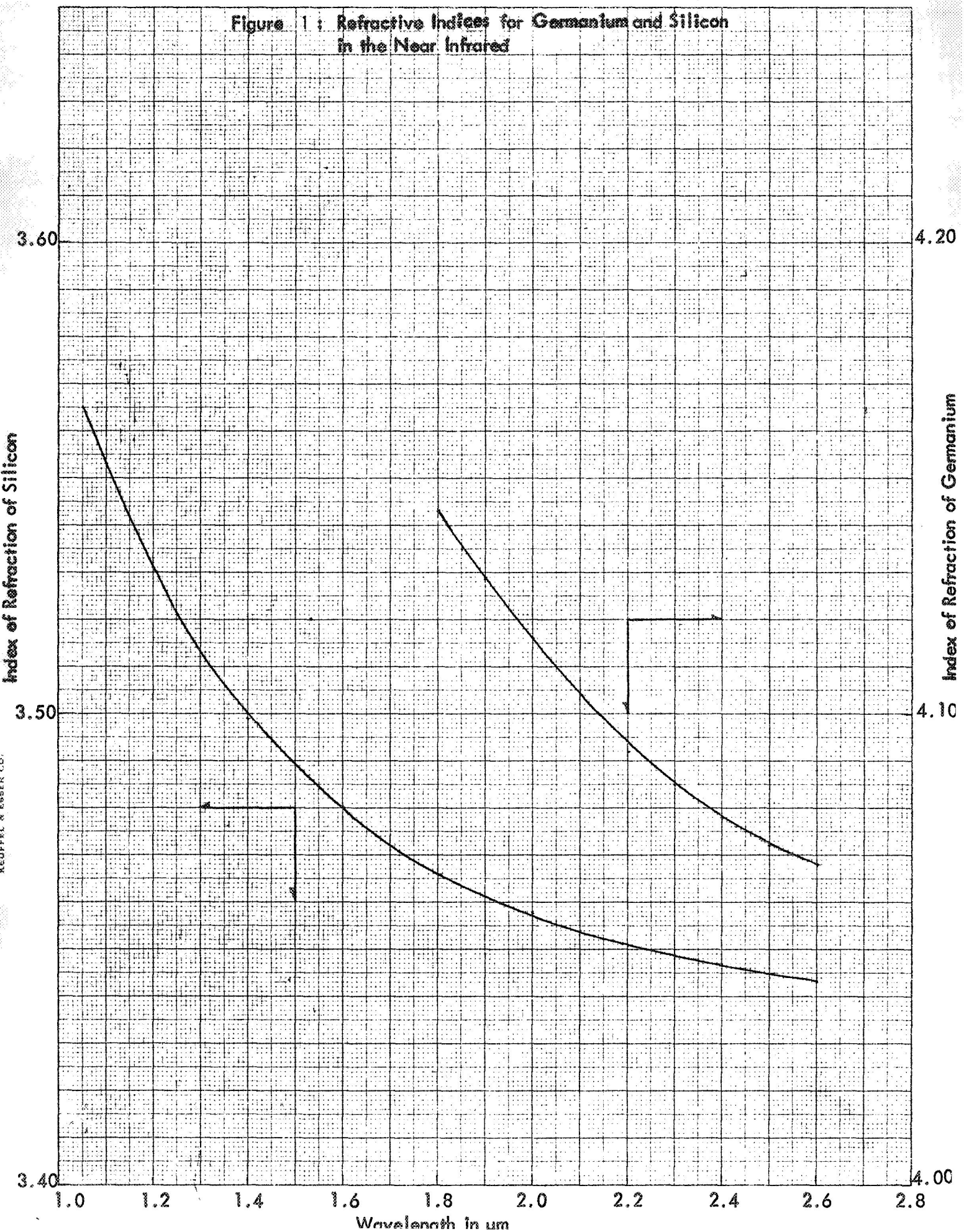
25) Barer, Cole and Thompson, Nature 163, 198 (1949)

26) D. L. Wood, Rev. Sc. Instr. 21, 764 (1950)

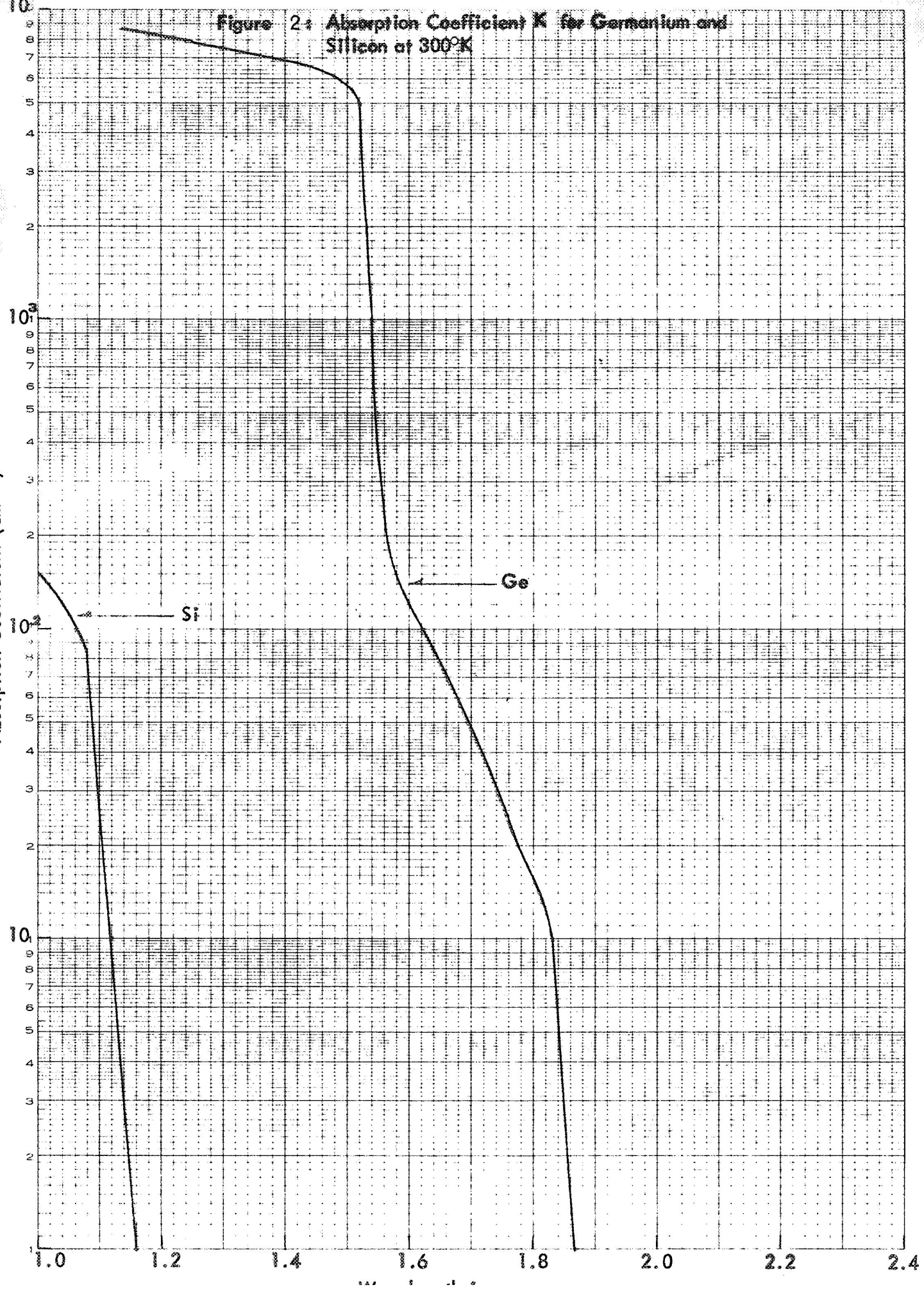
27) E. L. Schlegel, Rev. Sc. Instr. 34, 360 (1963)

28) B. R. Pagel and L. R. Reid, IEEE Trans, Instr. and Measur. p.89 (Sept 1966)

Figure 1 : Refractive Indices for Germanium and Silicon in the Near Infrared

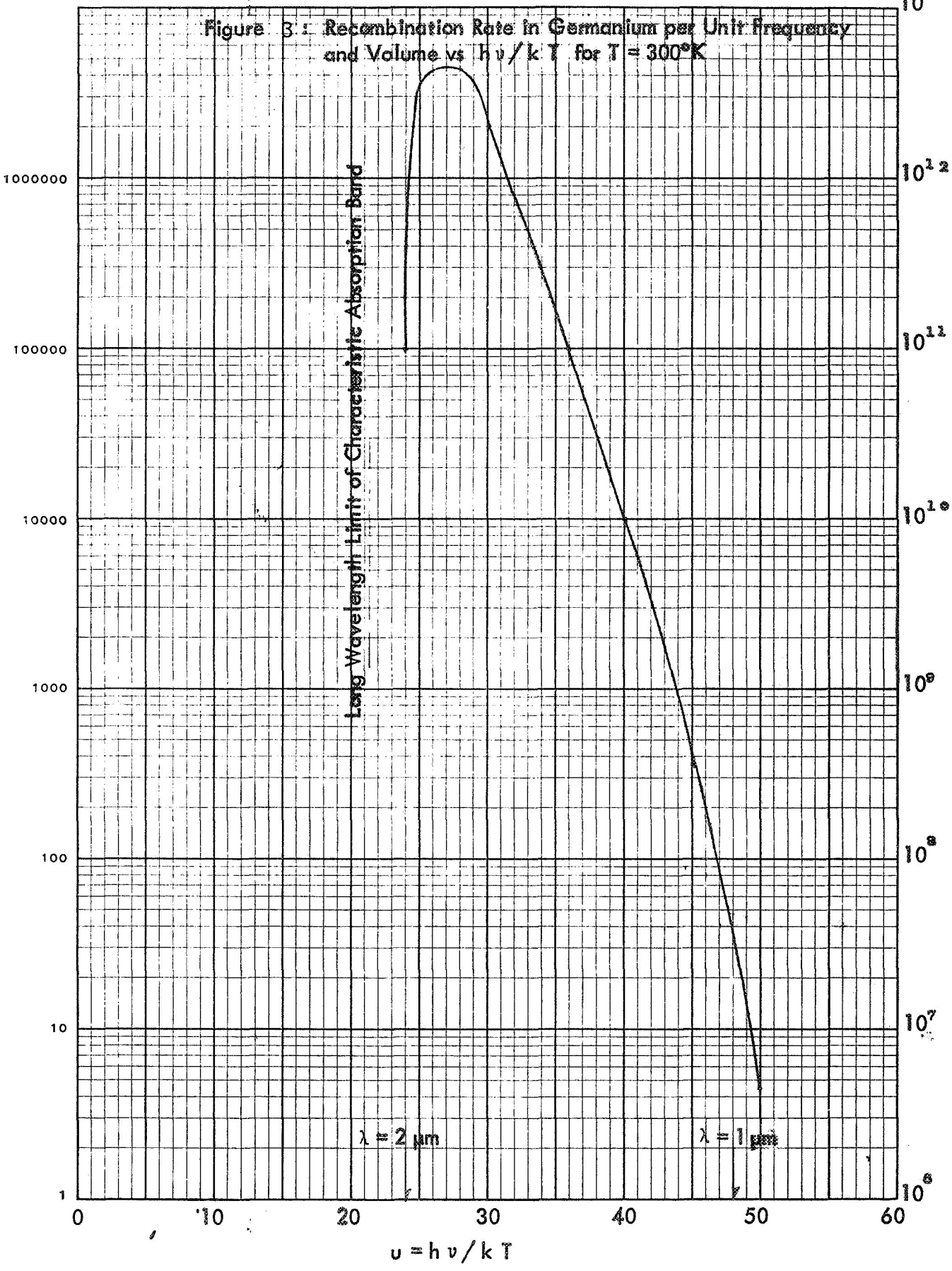


KEUFFEL & ESSER CO.


Figure 2: Absorption Coefficient K for Germanium and Silicon at 300°K
Absorption Coefficient (cm⁻¹)
Ge
Si
1.0
1.2
1.4
1.6
1.8
2.0
2.2
2.4
SEMI-LOGARITHMIC
4 CYCLES × 10 DIVISIONS PER INCH

MODEL DATE

Figure 3: Recombination Rate in Germanium per Unit Frequency and Volume vs $h\nu / kT$ for T = 300°K



KEUFFEL & ESSER CO
7 CYCLES X 60 DIVISIONS

Figure 4: Transmission of Plastic and Glass Fibers between 0.4 - 2 μm

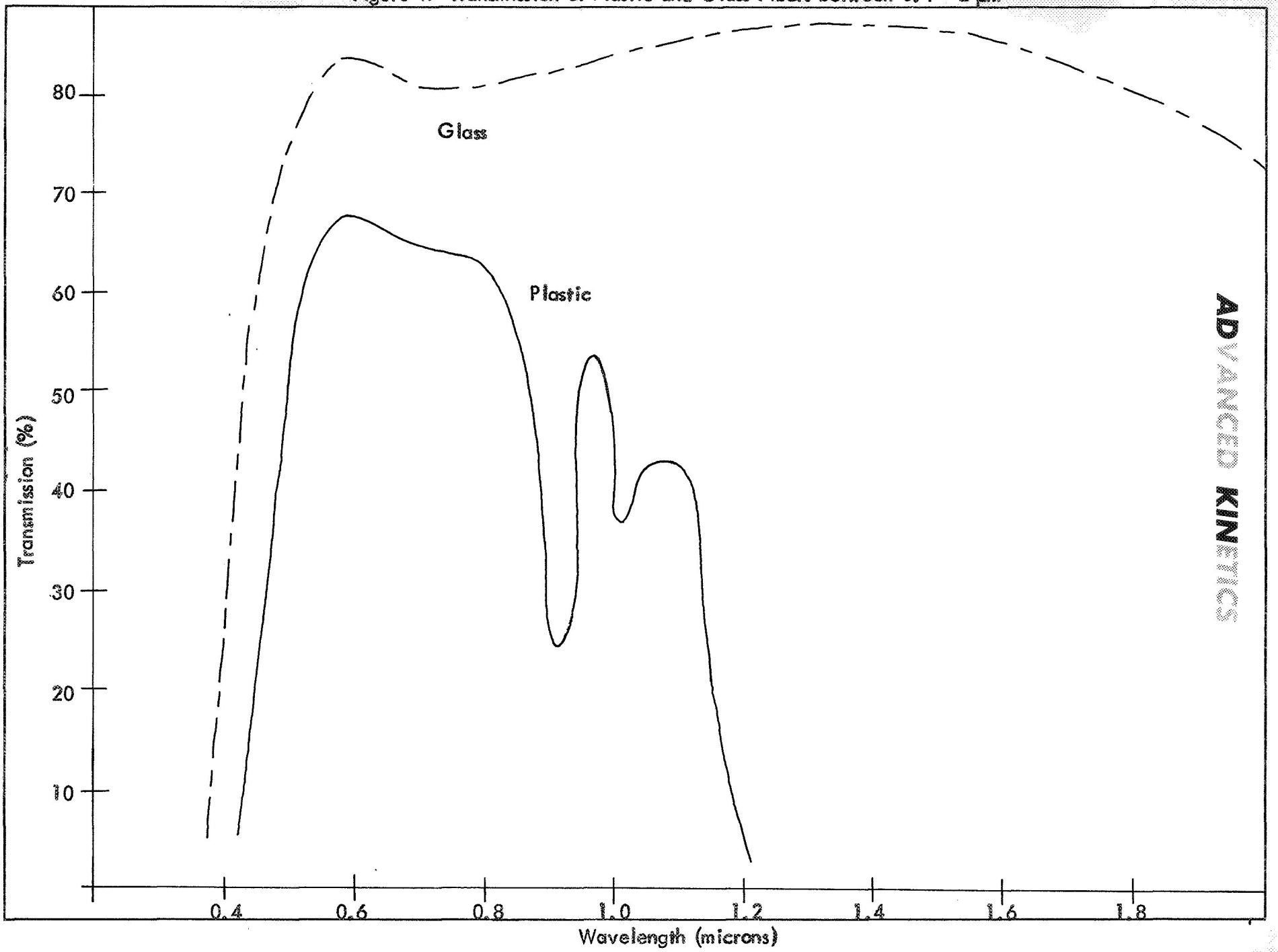
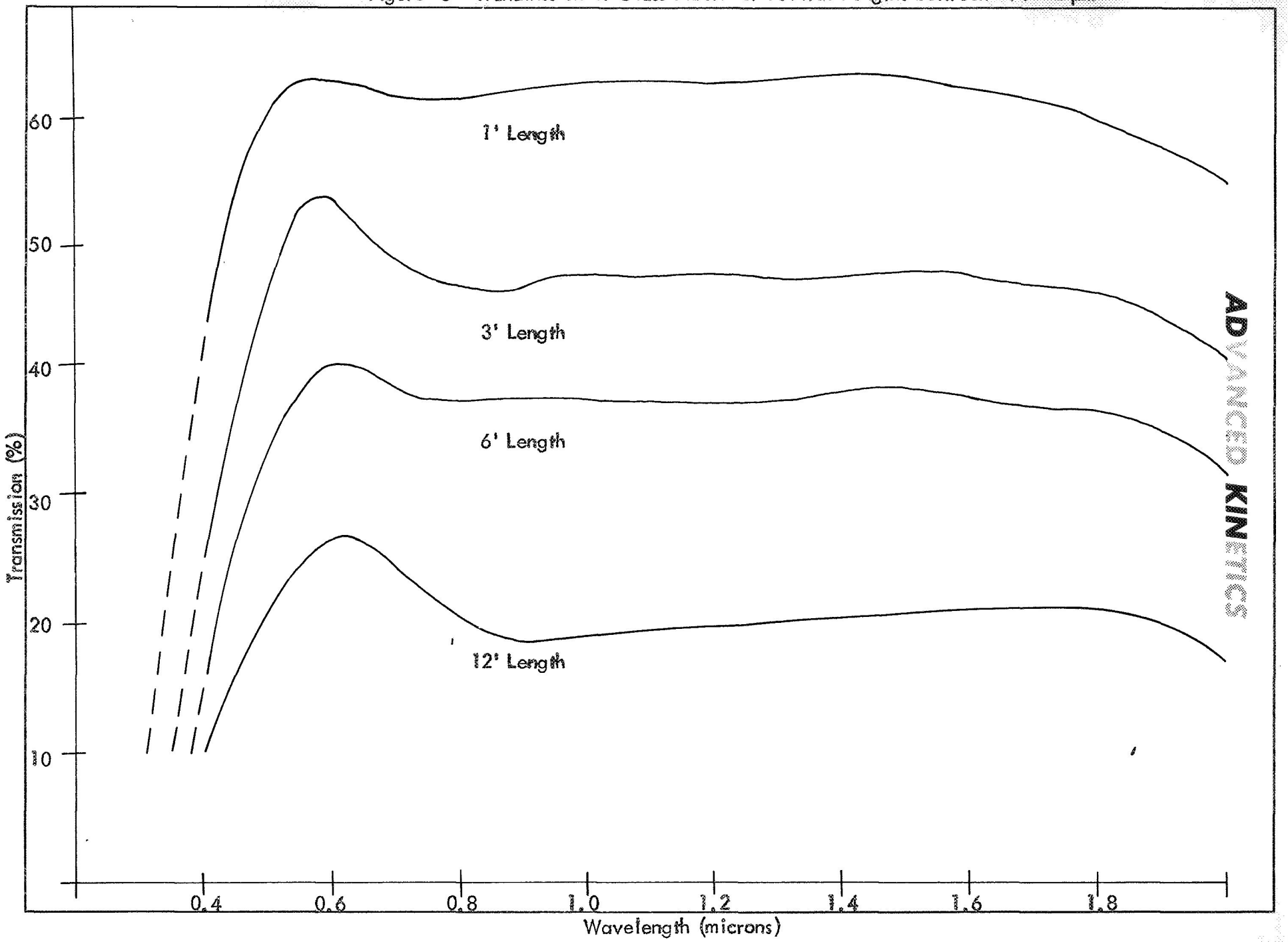


Figure 5: Transmission of Glass Fibers for Several Lengths between 0.4 – 2 μm



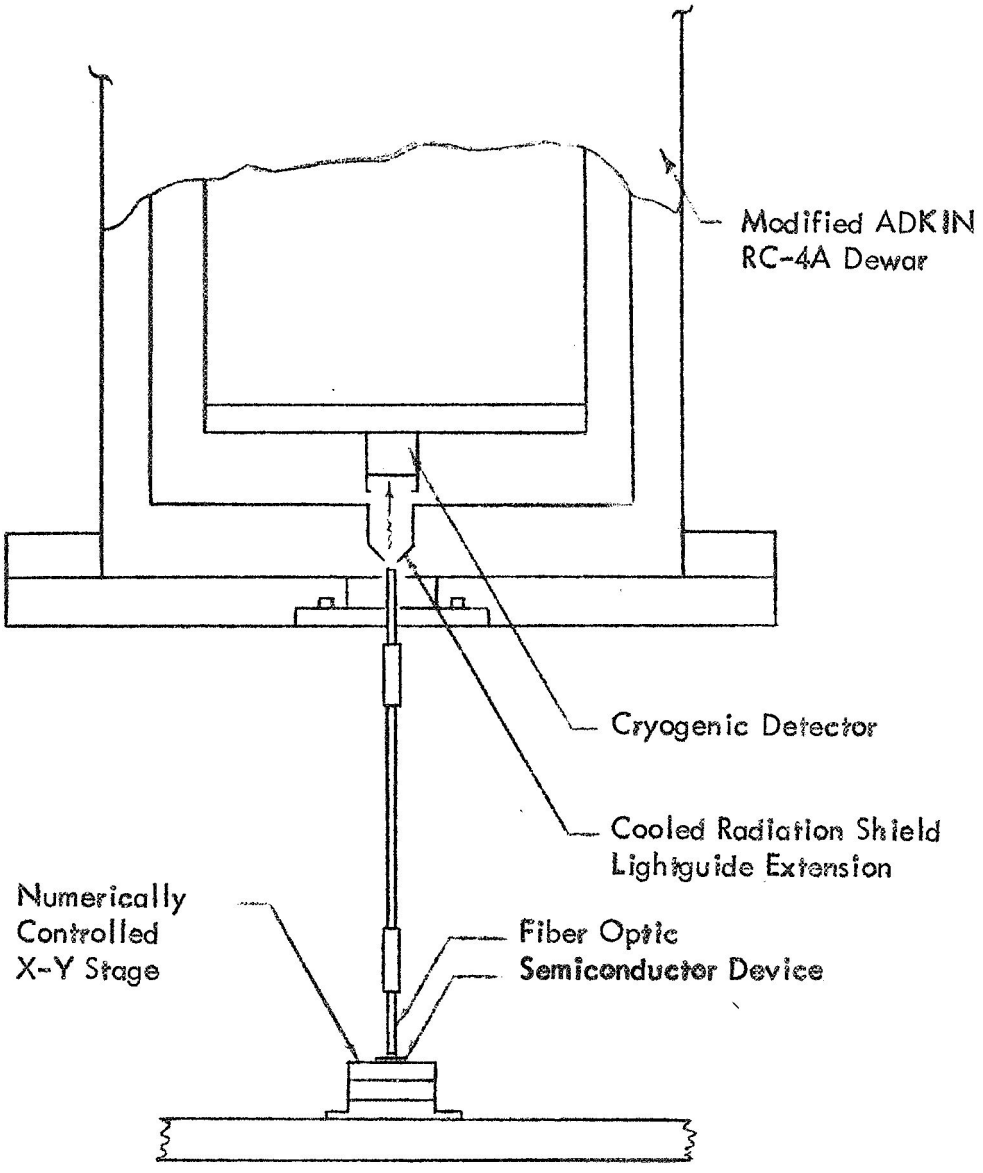


Figure 6: Experimental Configuration with Dielectric Lightguide

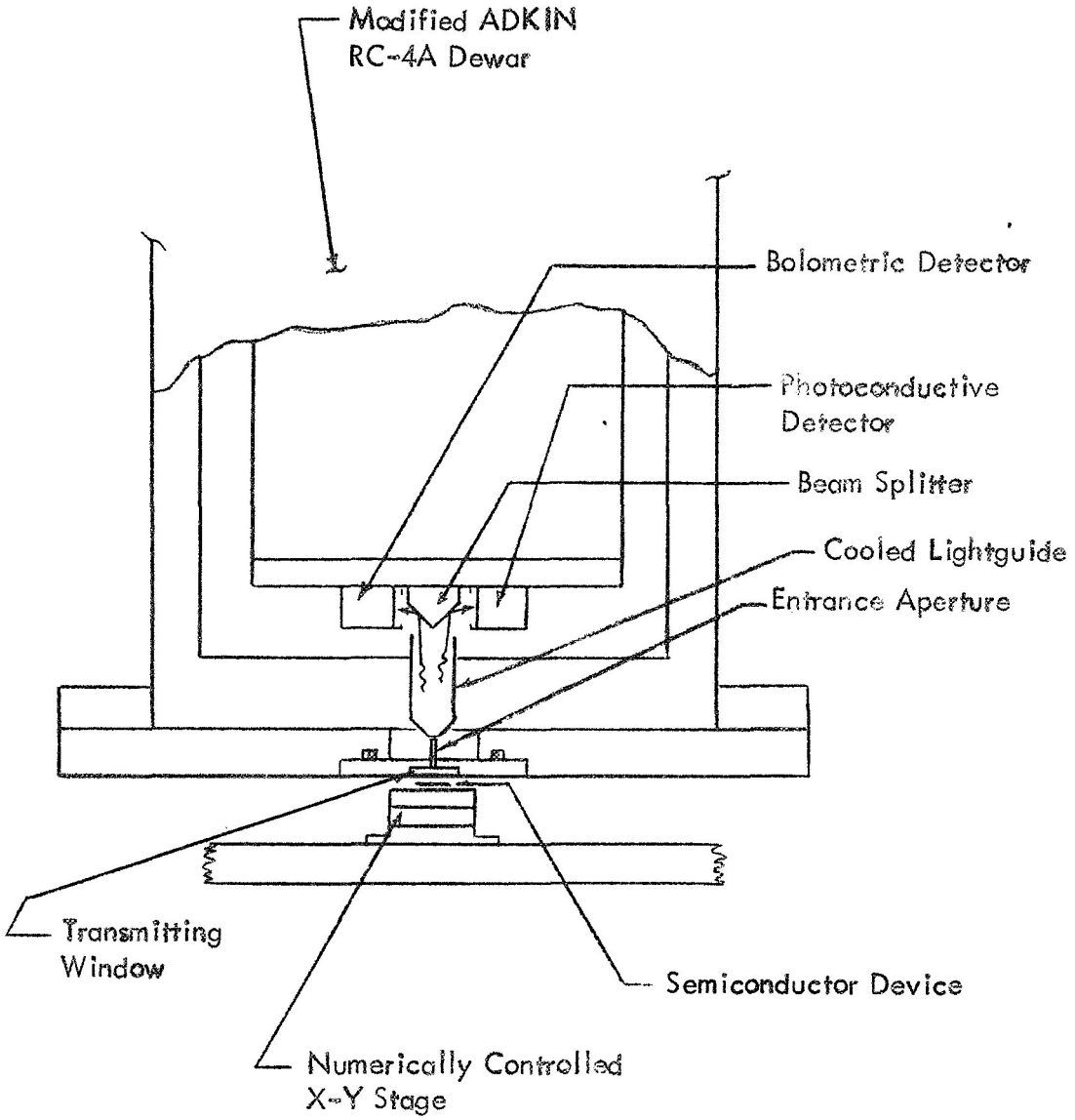


Figure 7: Experimental Configuration with Metallic Lightguide and Dual Detector

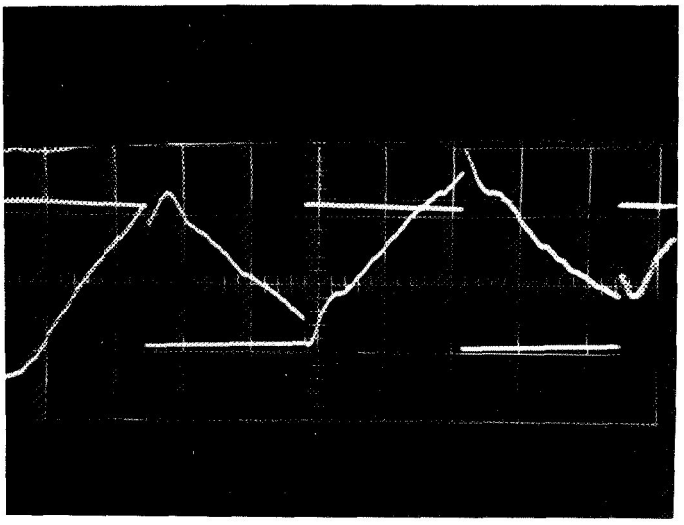


Figure 8: Radiation from 2N1183 NPN Power Transistor with Current Modulation Function

Time Base	2 msec/cm
Repetition Rate	100 pps
Current Amplitude	1 amp/cm
Signal Voltage	200 μv/cm

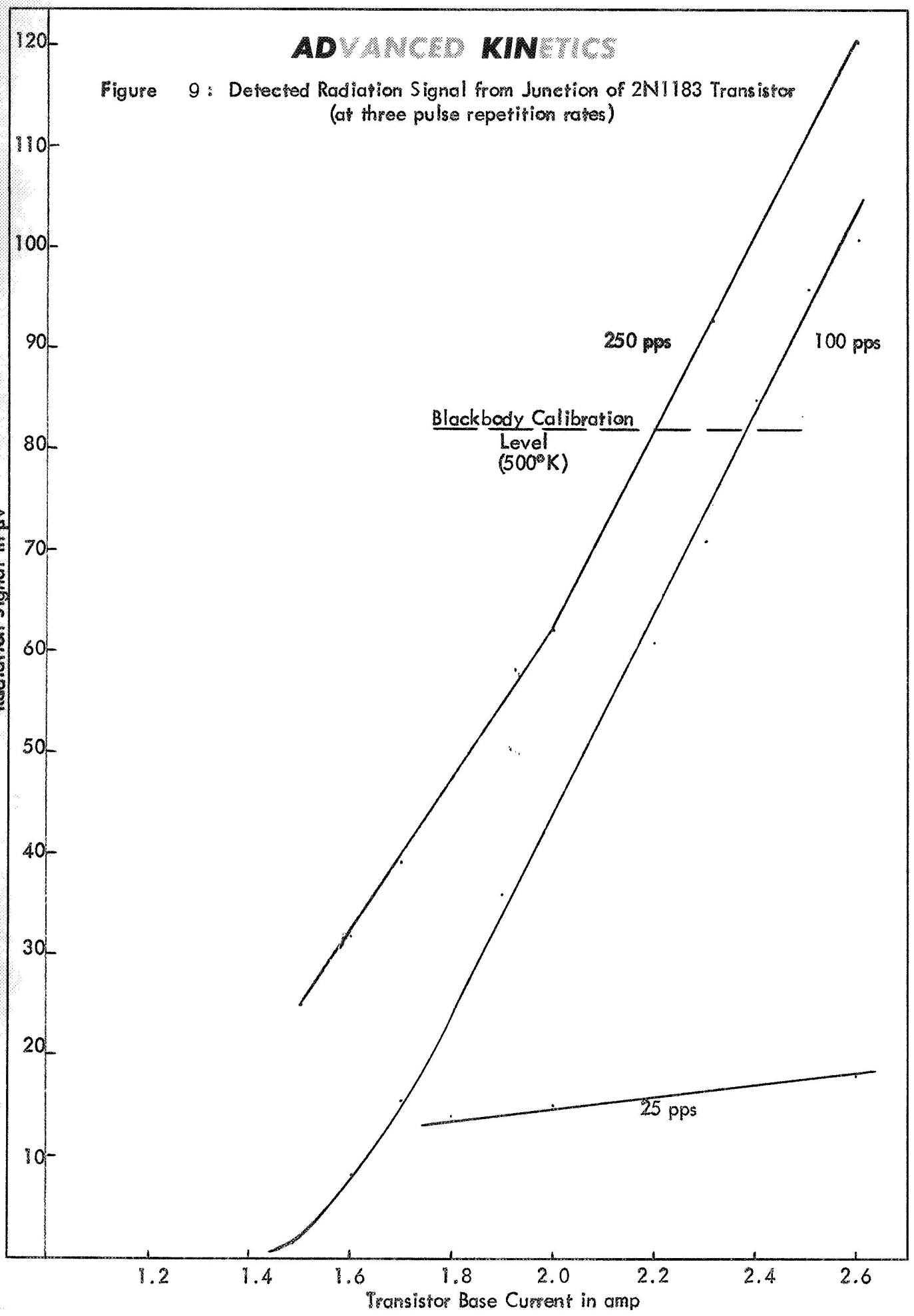
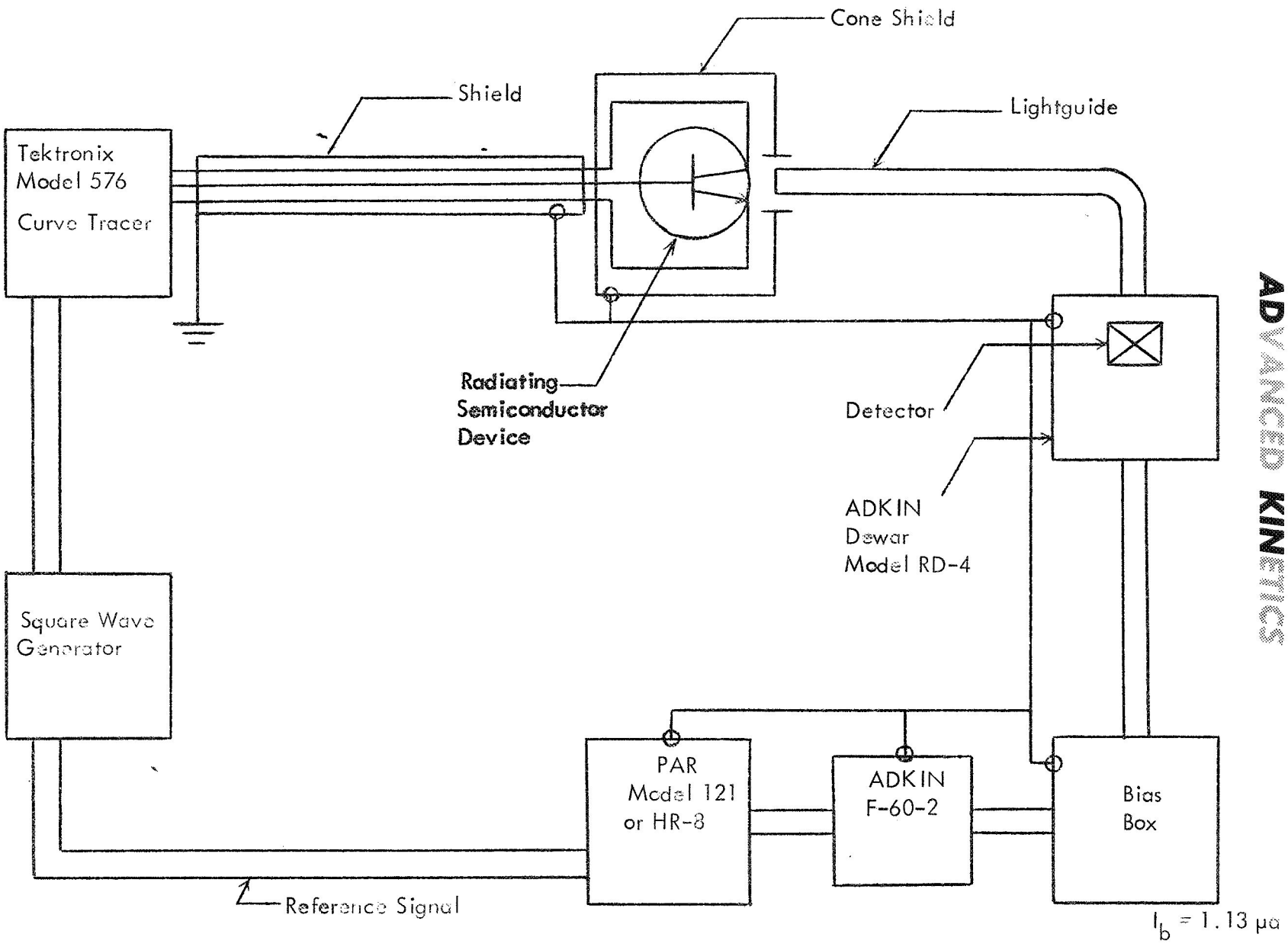

ADVANCED KINETICS
Figure 9 : Detected Radiation Signal from Junction of 2N1183 Transistor
(at three pulse repetition rates)
120
110
100
90
80
70
60
50
40
30
20
10
Radiation Signal in μv
250 pps
100 pps
Blackbody Calibration
Level
(500°K)
25 pps
1.2
1.4
1.6
1.8
2.0
2.2
2.4
2.6
Transistor Base Current in amp

Figure 10: Test Set-up for Measurement of Radiation from Semiconductors



ADVANCED KINETICS

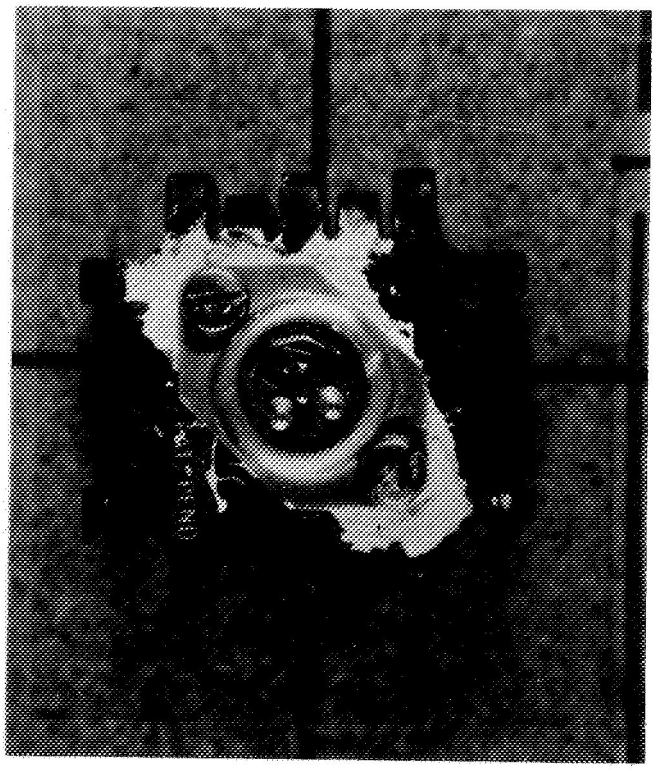


Figure 11a

Top View of NPN Power Transistor Type 2N 1701

Mounted on Heat Sink

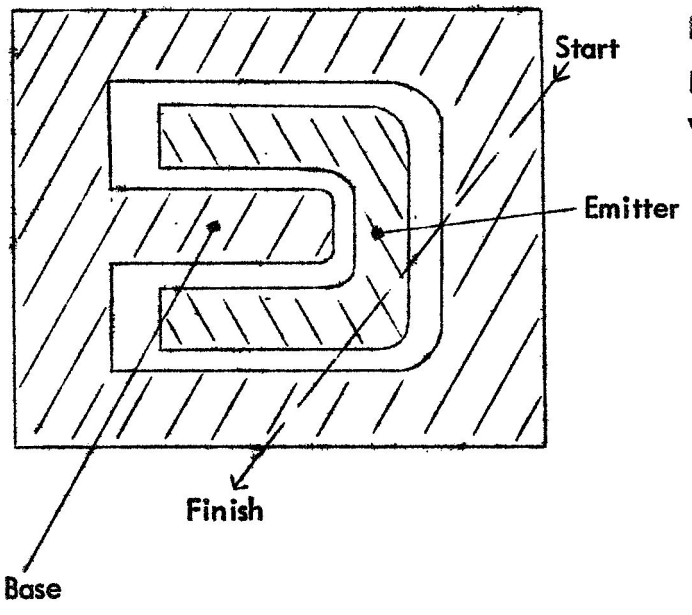


Figure 11b

Enlarged Drawing of NPN-2N1701 with Scan Line Entered

KEUFFEL & ESSER CO.

ADVANCED KINETICS, INC.

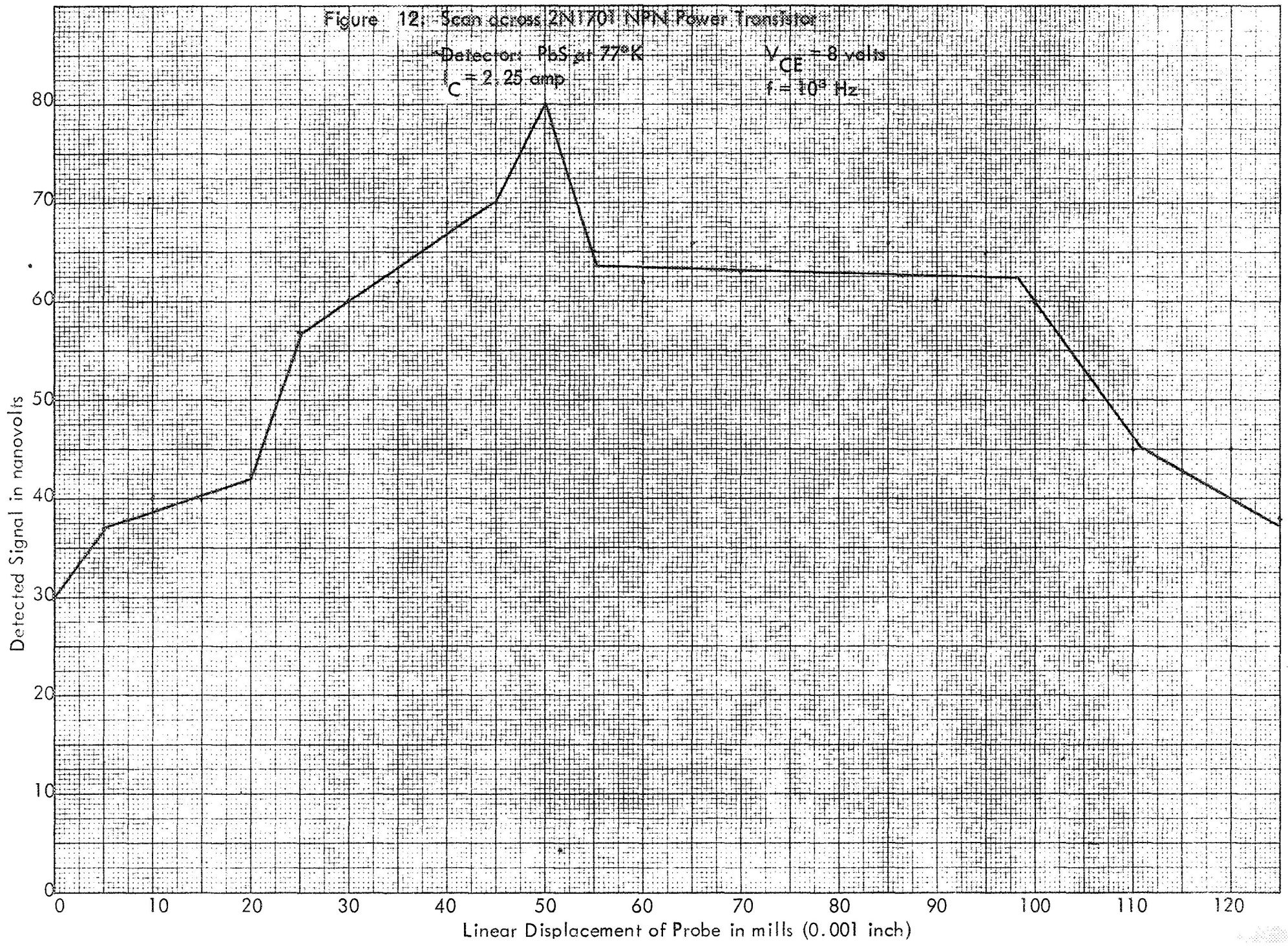


Figure 13: Numerically Controlled Stage Scan across Emitter-Base Junction of NPN-2N1701 Power Transistor

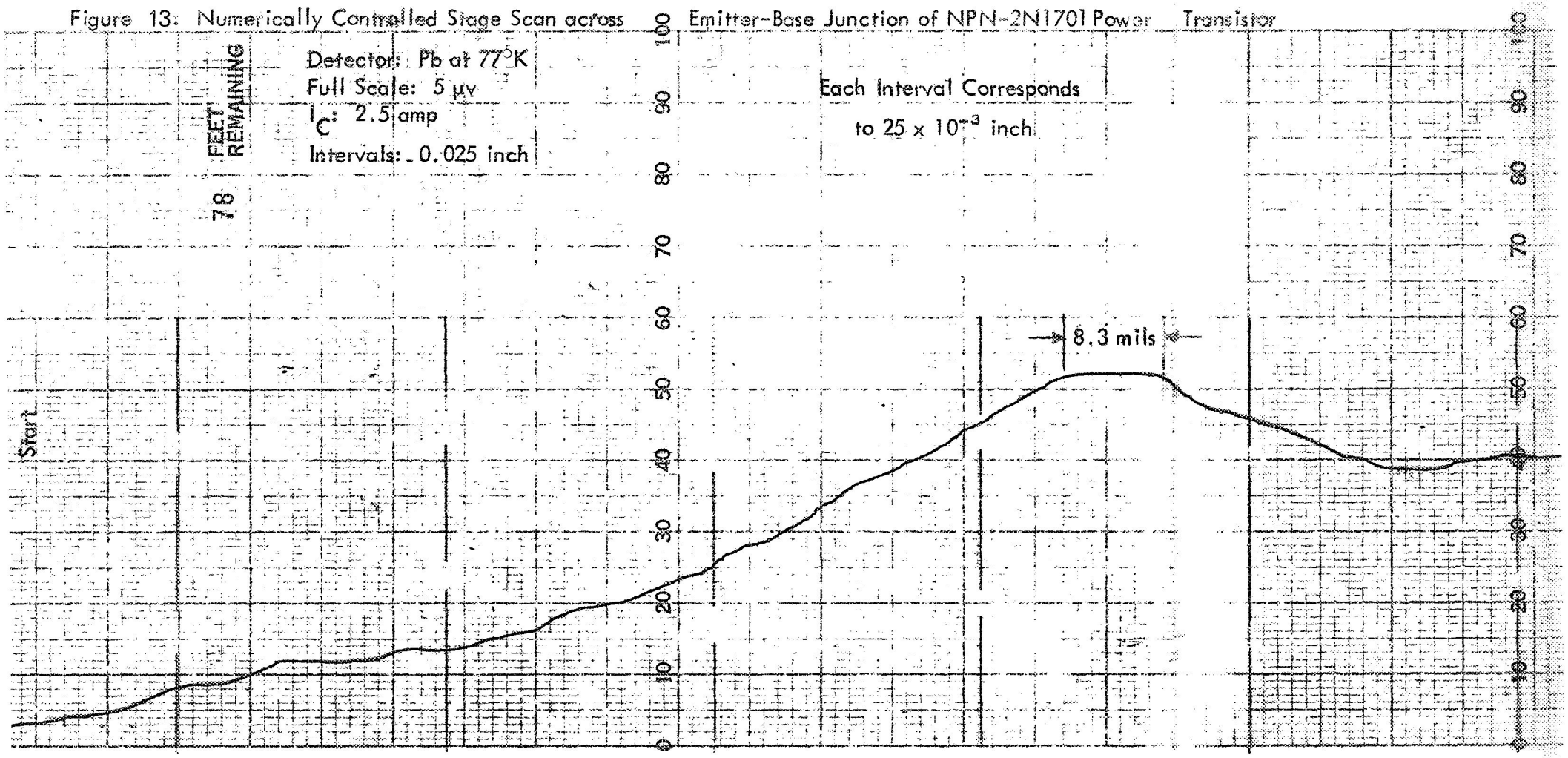
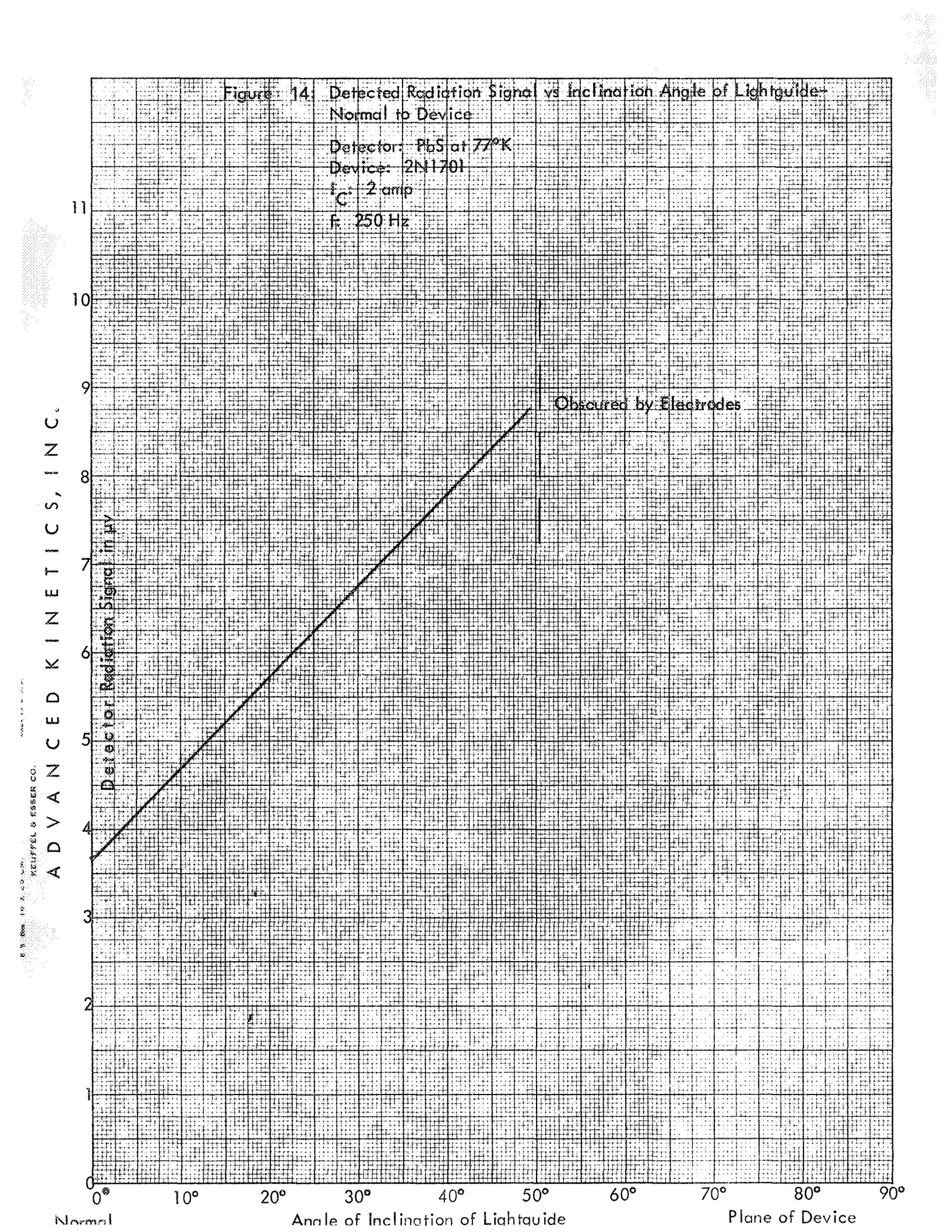


Figure 14: Detected Radiation Signal vs Inclination Angle of Lightguide-Normal to Device

Detector: PbS at 77°K
Device: 2N1701
I_C: 2 amp
F: 250 Hz



ADVANCED KINETICS, INC.
KEUFFEL & ESSER CO.

Figure 15: Detected Radiation Signal vs. Collector Current for NPN-2N1701 Power Transistor

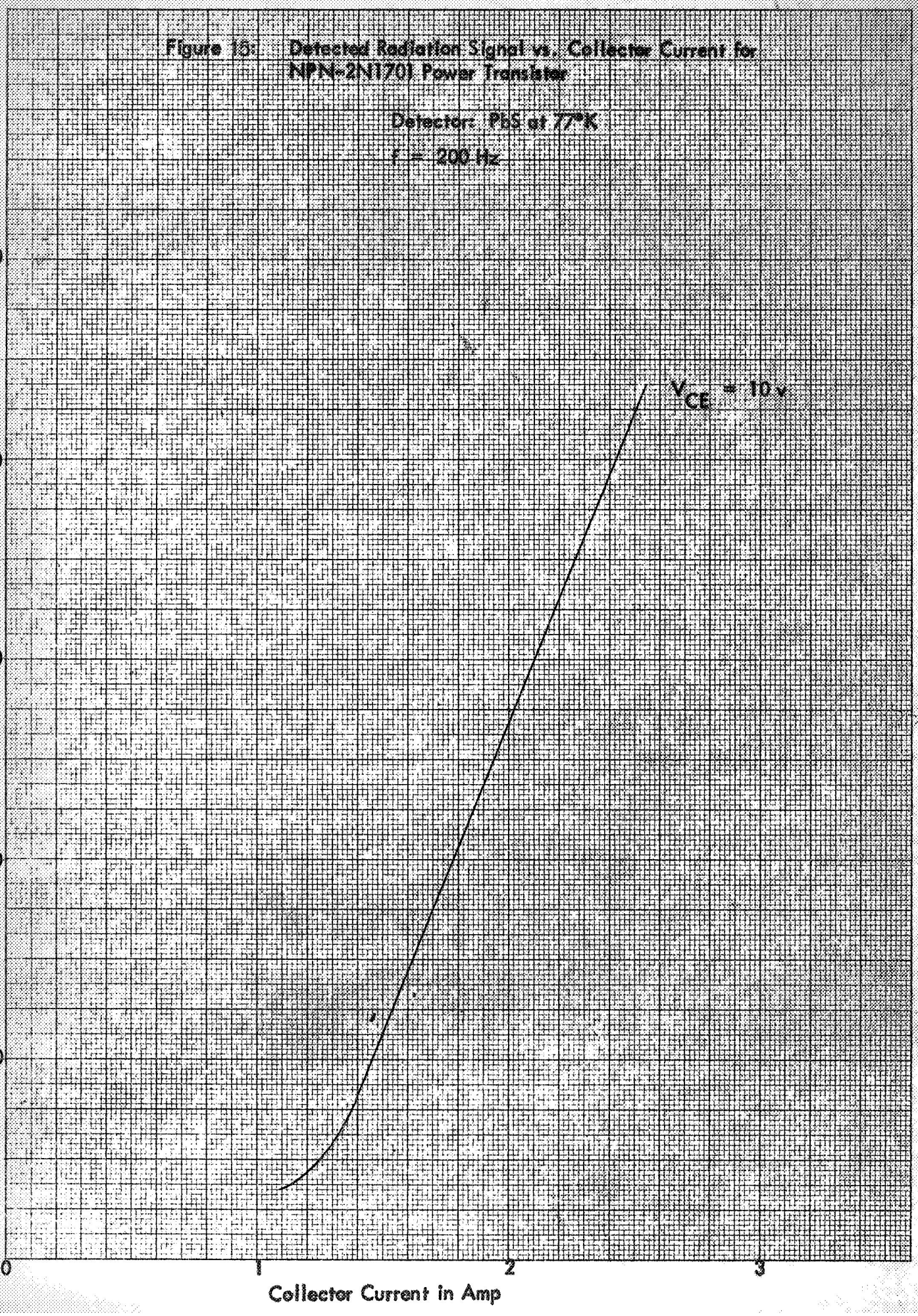


Figure 10: Detected Radiation Signal vs. Collector Voltage for NPN-2N1701 Power Transistor

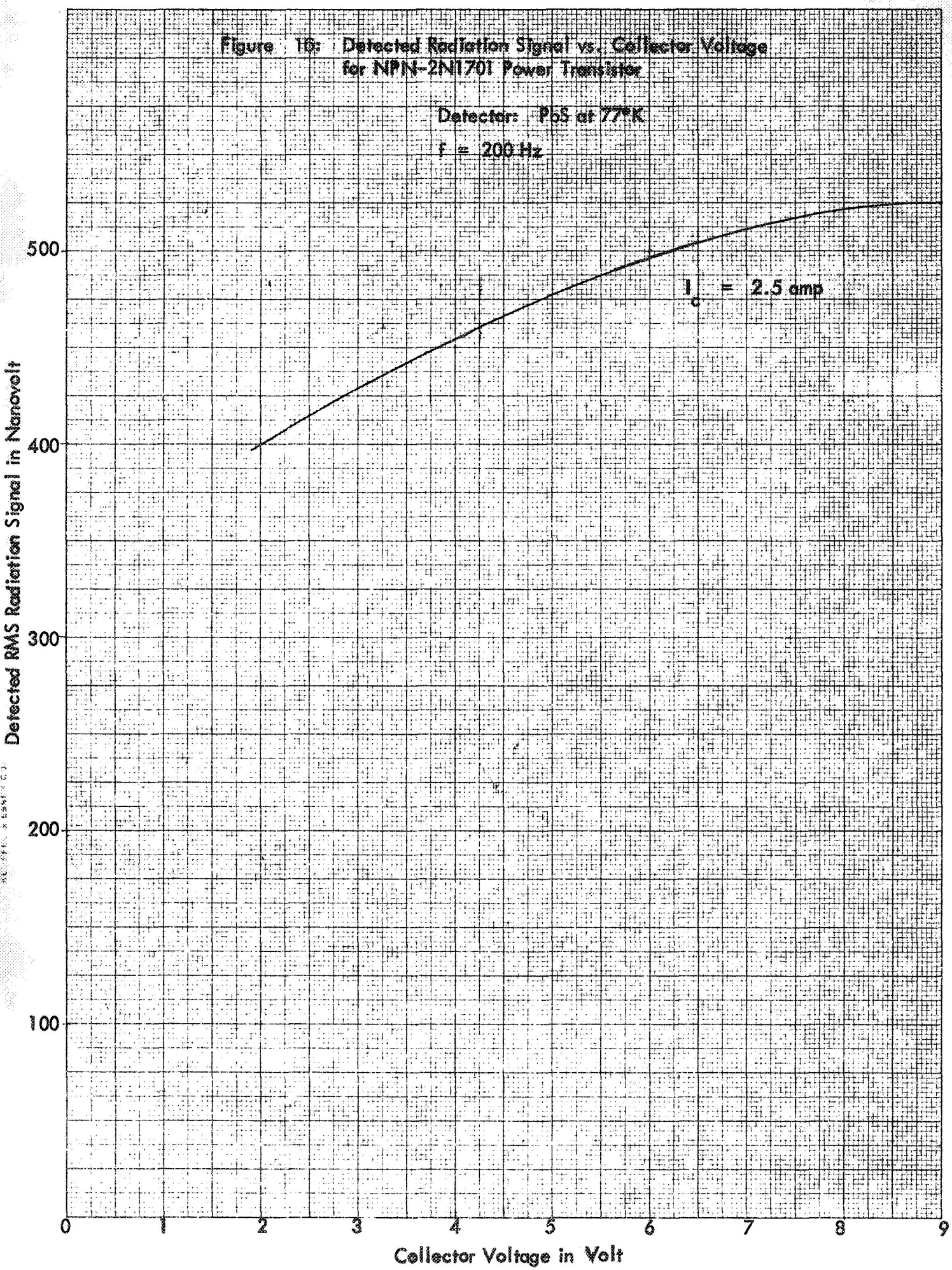
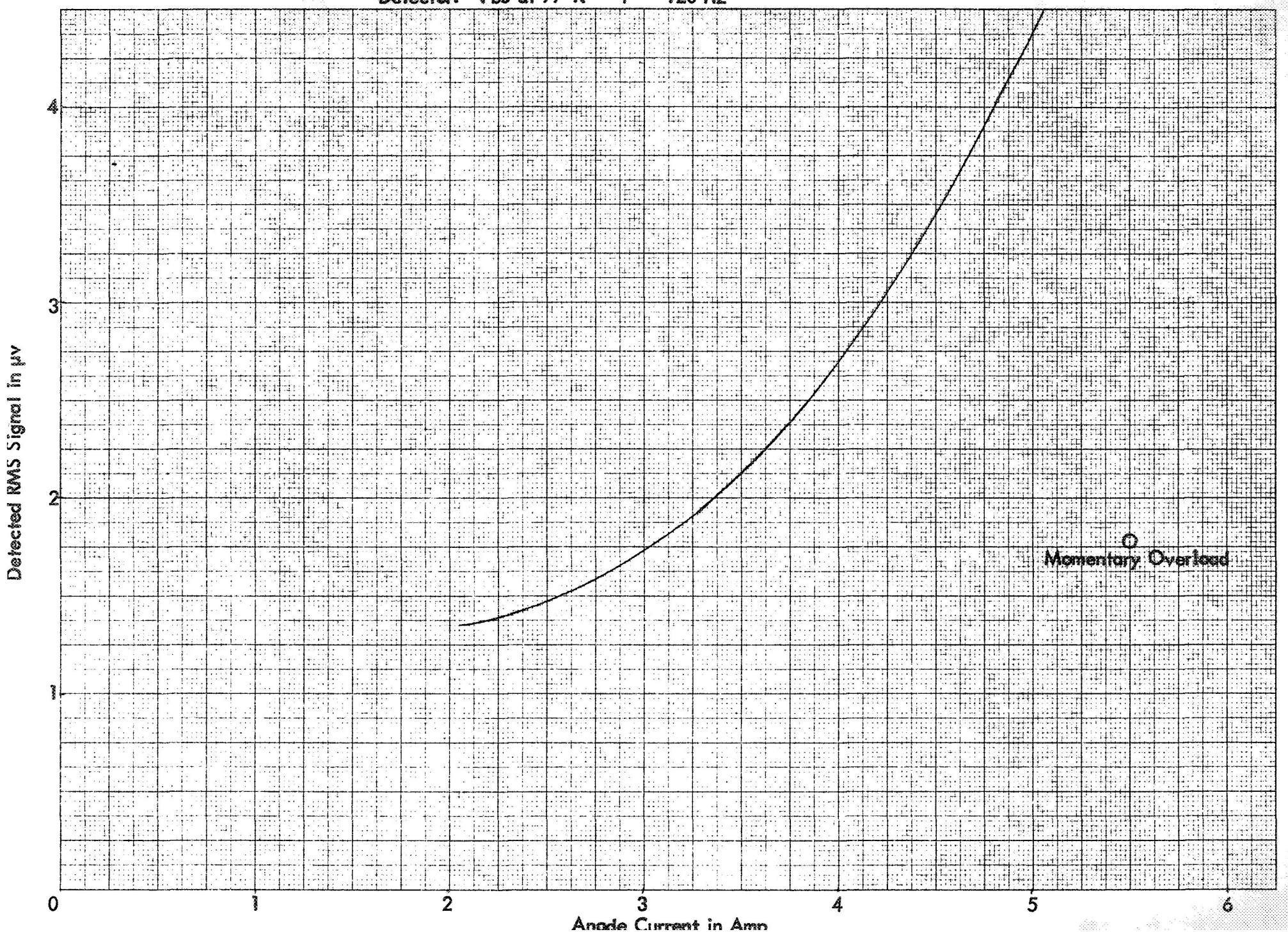


Figure 17: Detected Radiation Signal vs. Anode Current for RCA Triac 40430
Detector: PbS at 77°K f = 120 Hz



ADVANCED KINETICS, INC.

TABLE I

CALIBRATION OF PbS DETECTOR

T = 77°K

Bias Current - I_b	.5 μa	1 μa	2 μa	5 μa	10 μa
R (v/w)	$.663 \times 10^6$	2.97×10^6	$.288 \times 10^6$	$.092 \times 10^6$	$.052 \times 10^6$
NEP (w)	1.37×10^{-10}	8.25×10^{-11}	1.26×10^{-10}	2.69×10^{-10}	7.69×10^{-10}
NEP/$\sqrt{BW}$ (w/$Hz^{\frac{1}{2}}$)	4×10^{-11}	2.48×10^{-11}	3.79×10^{-11}	8×10^{-11}	2.31×10^{-10}
D^*_{bb} (cm $Hz^{\frac{1}{2}}$/w)	2.52×10^9	4.07×10^9	2.66×10^9	1.26×10^9	4.29×10^8

T = 4.2°K

Bias Current - I_b	.1 μa	.2 μa	.5 μa	1 μa
R (v/w)	19.3×10^8	36.5×10^8	66.2×10^8	16.6×10^8
NEP (w)	5×10^{-10}	2.64×10^{-10}	1.46×10^{-10}	5.81×10^{-10}
NEP/$\sqrt{BW}$ (w/$Hz^{\frac{1}{2}}$)	1.52×10^{-10}	8.0×10^{-11}	4.4×10^{-11}	1.76×10^{-10}
D^*_{bb} (cm $Hz^{\frac{1}{2}}$/w)	6.5×10^8	1×10^9	2.27×10^9	5.681×10^8

ADVANCED KINETICS

TABLE II

CALIBRATION OF Ge:Hg DETECTOR

T = 77°K						
Bias Current - I_b	1 μa	5 μa	10 μa	50 μa	100 μa	200 μa
R (v/w)	34	122	175	243.4	321	292
NEP (w)	1.68×10^{-7}	4.7×10^{-8}	5.7×10^{-8}	8.8×10^{-8}	11.1×10^{-8}	18.3×10^{-8}
NEP/$\sqrt{BW}$ (w/Hz$^{\frac{1}{2}}$)	1.24×10^{-8}	346×10^{-9}	4.23×10^{-9}	6.5×10^{-9}	8.2×10^{-9}	13×10^{-9}
D^*_{bb} (cm Hz$^{\frac{1}{2}}$/w)	1.6×10^{7}	5.78×10^{7}	4.7×10^{7}	3.66×10^{7}	2.43×10^{7}	1.47×10^{7}

T = 4.2°K			
Bias Current - I_b	1 μa	2 μa	5 μa
R (v/w)	560	995	798
NEP (w)	9×10^{-11}	2×10^{-10}	2.5×10^{-10}
NEP/$\sqrt{BW}$ (w/Hz$^{\frac{1}{2}}$)	2.8×10^{-11}	6.06×10^{-11}	7.58×10^{-11}
D^*_{bb} (cm Hz$^{\frac{1}{2}}$/w)	7×10^{9}	3×10^{9}	2.34×10^{9}

ADVANCED KINETICS